



Neocortical Slow Oscillations Implicated in the Generation of Epileptic Spasms

Chih-hong Lee, MD^{1,2,5}, John T. Le^{2,3}, BS, Carlos J. Ballester-Rosado, PhD^{2,3}, Anne E. Anderson, MD^{1,2,3,4} & John W. Swann, PhD^{1,2,3}

¹Department of Neuroscience, Baylor College of Medicine, Houston, Texas, USA

²The Cain Foundation Laboratories, The Jan and Dan Duncan Neurological Research Institute, Texas Children's Hospital, Houston, Texas, USA

³Department of Pediatrics, Baylor College of Medicine, Houston, Texas, USA

⁴Department of Neurology, Baylor College of Medicine, Houston, Texas, USA

⁵Department of Neurology, Chang Gung Memorial Hospital Linkou Medical Center and Chang Gung University College of Medicine, Taoyuan, Taiwan

Correspondence should be addressed to: John W. Swann Ph.D.

The Jan and Dan Duncan Neurological Research Institute

1250 Moursund St. Suite 1225, Houston, TX77030

(ph.) 832-824-3969

This article has been accepted for publication and undergone full peer review but has not been through the copyediting, typesetting, pagination and proofreading process which may lead to differences between this version and the Version of Record. Please cite this article as doi: 10.1002/ana.25935

email: jswann@bcm.edu

Running head: Neocortical Oscillations and Spasms

Number of characters in the Title: 78

Number of characters in the Running Head: 35

Number of words in the Abstract: 243

Number of words in the Introduction: 648

Number of words in the Discussion: 1225

Number of words in the body of the Manuscript: 7150

Number of Figures: 8

Accepted Article

Abstract

Objective: Epileptic spasms are a hallmark of severe seizure disorders. The neurophysiological mechanisms and the neuronal circuit(s) that generate these seizures are unresolved and are the focus of studies reported here.

Methods: In the tetrodotoxin model, we used 16-channel microarrays and microwires to record electrophysiological activity in neocortex and thalamus during spasms. Chemogenetic activation was used to examine the role of neocortical pyramidal cells in generating spasms. Comparisons were made to recordings from infantile spasms patients.

Results: Current source density and simultaneous multiunit activity analyses indicate that the ictal events of spasms are initiated in infragranular cortical layers. A dramatic pause of neuronal activity was recorded immediately prior to the onset of spasms. This preictal pause is shown to share many features with the down states of slow-wave sleep. In addition, the ensuing interictal up states of slow-wave rhythms are more intense in epileptic than control animals and

occasionally appear sufficient to initiate spasms. Chemogenetic activation of neocortical pyramidal cells supported these observations since it increased slow oscillations and spasm numbers and clustering. Recordings also revealed a ramp-up in the number of neocortical slow oscillations preceding spasms, which was also observed in infantile spasms patients.

Interpretation: Our findings provide evidence that epileptic spasms can arise from the neocortex and reveal a previously unappreciated interplay between brain state physiology and spasm generation. The identification of neocortical up states as a mechanism capable of initiating epileptic spasms will likely provide new targets for interventional therapies.

Introduction

Epileptic spasms are brief and sudden flexion or extensions of the head, limbs and/or axial muscles. They are most frequently observed during infancy when they are referred to as infantile spasms¹. However, they have been reported to persist well beyond infancy²⁻⁴ and in up to 19% of patients^{5, 6}. Numerous studies have also reported epileptic spasm onset in older children and adults⁷⁻¹⁰. Some of the clinical features of infants and older patients with spasms are different. For instance, hypsarrhythmia, the chaotic interictal EEG pattern of infantile spasms is seen much less frequently in older patients whether they had spasms as infants or not^{2-4, 7-9}. However, one feature shared by epileptic spasm patients are the brief behavioral spasms that occur in clusters and the concurrent EEG ictal event^{2-4, 7-9, 11}. In the various epileptic spasms' patient populations,

the ictal event consists of a large initiating slow wave, followed by a marked attenuation of EEG amplitude called an electrodecrement. The neuronal mechanisms that produce these ictal events are unresolved but once understood should impact our understanding of the pathophysiology of spasms across ages.

Very little is known definitively about the areas of the brain that generate epileptic spasms. Most information comes from studies of infantile spasms since it is a much larger patient population and consequently studied more. One prevailing idea is that the spasms are likely produced by interactions between abnormal cortical and subcortical circuits¹². Reasons to suspect brainstem involvement include disturbances in sleep-wake cycles¹³ and similarities between the Moro reflex in infants and epileptic spasms¹⁴. One reason the cortex has been proposed as a generator is that some children with spasms have discrete cortical lesions with no other recognizable brain pathology. Results from PET studies have shown focal metabolic abnormalities in the cortex with normal MRI results¹⁵, and epileptic spasms have been eliminated in some children when the PET-identified focus was surgically removed¹⁶⁻¹⁹. Based on this, it has been proposed that epileptic spasms likely originate in the cortex and the contribution of the brainstem is secondary to the cortical discharges²⁰.

In an animal model of epileptic spasms, recordings from the neocortex have consistently revealed high frequency oscillations (HFOs) at the onset of spasms that are concurrent with a burst of multiunit activity (MUA)²¹. Since HFOs are thought to be electrophysiological biomarkers for epileptogenic brain circuits^{22, 23}, these results coupled with the observed unit

Accepted Article

firing suggest that the neocortex at least participates in the generation of spasms. Moreover, interictal HFOs have also been reported to be most frequent during non-rapid eye movement (NREM) sleep^{21, 24}. This raises the possibility that the neocortical mechanisms that underlie this sleep state could predispose the neocortex to generate epileptiform activity and possibly spasms. During NREM sleep, rhythmic slow waves occur simultaneously with dramatic alterations in the activity of individual neurons called up and down states²⁵⁻²⁹. Extracellular unit firing is markedly increased during up states and dramatically silenced during down states and each cycle is concurrent with the generation of a slow wave in local field potential (LFP) recordings. These changes in brain states are thought by many to originate in the neocortex although there is evidence for thalamic involvement as well^{26, 30-32}.

Our laboratory has developed a rat model with robust epileptic spasms through chronic infusion of the sodium channel blocker, tetrodotoxin (TTX) into the cortex beginning on postnatal days 10-12 (P10-12)³³. Within 1 week, animals begin to have flexion or extension spasms of the trunk and forelimbs which persist for 2-3 months. TTX has also been shown to produce a lesion at its infusion site²⁴ which likely recapitulates the acquired structural brain abnormalities observed in many patients³⁴. In experiments reported here, we took advantage of this model to test the hypothesis that epileptic spasms can be initiated through the activity of neocortical pyramidal cells. We also examined the role alterations in the up and down states play in the generation of spasms.

Materials and Methods

All procedures reported here were approved by the Baylor College of Medicine Institutional Animal Care and Use Committee and were in keeping with NIH guidelines. All surgeries were done under isoflurane anesthesia.

TTX Model of Epileptic Spasms

To produce the TTX model of epileptic spasms, 11-day-old Wistar rat pups were implanted with an osmotic mini-pump (Alzet) containing 200 μ l of 12 μ M TTX. Both male and female were used. The pump was connected to a cannula that was stereotaxically implanted into the right neocortex. The pump provided a continuous infusion of the TTX solution at a rate of about 0.25 μ l/h. The implantation location was 2 mm lateral to the midline (ML), 2.2 mm posterior to the Bregma (AP), and 1.5 mm deep into the cortex (DV). After recovery from anesthesia, the pups were monitored for behavioral spasms. About 30-50% of the pups developed spasms. The spasms usually began on P16 or a few days later.

Electrode Implantation and Neurophysiological Data Acquisition

For multielectrode array experiments, a 16-channel silicon probe (NeuroNexus, 100 μ m intervals) attached to a microdrive (NeuroNexus dDrive-m) was implanted on P39-50, into the left somatosensory cortex contralateral to the TTX infusion site (-2 mm AP, -2.5 mm ML, 0.6 mm DV). On the day of recordings, the tip of the silicon probe was advanced into the cortex with a dDrive-m to the target position where neuronal spikes could be easily recorded (about 1800 μ m

Accepted Article

deep). For the thalamic recording experiment, perfluoroalkoxy (PFA)-coated tungsten wires (bare diameter 50.8 μm , A-M Systems) were inserted into a 33-gauge stainless steel guiding tubing (Plastics One), then implanted bilaterally into ventrobasal complex (-2.6 mm AP, 2.7-2.8 mm ML, 5.8 mm DV). Another six PFA-coated tungsten wires were implanted bilaterally into cortices (**Fig 3A**); recording electrodes were implanted 1.2 mm below the cortical surface. The eight tungsten wires were connected to an electrode interface board (Neuralynx EIB-18). Two screws in the skull overlying the cerebellum served as ground and reference electrodes. Neurophysiological signals were amplified and sampled at 30 kHz by the Neuralynx Cheetah32 system using a headstage directly attached to the silicon probe or EIB-18. As with the clinical settings, the input signals were inverted so that the negative potentials were upward. After the surgery, six-hours of video-EEG recordings were made for 1-5 days.

Current Source Density Analysis

CSD is a method of analysis of LFPs at multiple sites leading to estimates of the sites of the local generator of the measured potentials. Traditionally, CSD is computed as the second spatial derivative of the LFPs. During *in vivo* recordings, incidental neuronal activity originating from many sources impinge on the neurons from which recordings are made. In order to isolate the initial slow wave of ictal events, an independent component analysis (ICA) was first applied to the raw signals, and the independent component representative of the initial slow wave was extracted. Virtual LFPs produced by that component were reconstructed, and these LFPs were used to calculate the CSD³⁵. CSD analysis was computed by the standard method³⁶:

$$CSD_z = -\sigma_z \times \frac{\partial^2 \phi}{\partial z^2} \approx -\sigma_z \times \frac{\phi_{z+n\Delta z} - 2\phi_z + \phi_{z-n\Delta z}}{(n\Delta z)^2}$$

where σ is the conductivity, ϕ_z is the potential value at depth z , Δz is the spacing between adjacent electrodes, and $n\Delta z$ is the differentiation grid (in our case, $n = 1$).

MUA Analysis

For unit analysis, raw signals were first bandpass filtered (256th order finite impulse response, 600-9000 Hz), then the MUA spikes were extracted by Neuralynx Cheetah software with the amplitude threshold set at four times the standard deviation of the background signal amplitude. The background signals were taken from 10 s of recordings during waking without movement artifacts. The analysis periods for the spike firing rate and HFOs were 50 ms for the preictal pauses and interictal events and 200 ms for the ictal events throughout this paper. To make the peri-ictal time histogram (**Fig 2E** and **4D**), the MUA counts were first segregated into 10 ms bins, and the occurrence of the first spike of the ictal events was set as time 0. To determine the timing of MUA firing with regard to the phase of the LFP slow waves (**Fig 5C**), raw signals were bandpass filtered for slow wave oscillations (1-8 Hz); the instantaneous phase of these slow waves was calculated by Hilbert transform, then the timestamps of MUA were matched to the phase of the oscillations.

Up and Down State Analysis

The neocortical up and down states were defined from binned MUA counts³⁷. MUA spikes were counted in 10 ms bins and smoothed with a 30 ms Gaussian window. The smoothing prevented isolated spikes in silent periods from being classified as an up state. Bins with fewer than one spike count were considered silent. Consecutive silent bins above 50 ms were defined as one down state.

To compute the number of preictal down states per second (**Fig 5F**), first the ictal events were manually identified, but ictal events with preceding inter-spasm intervals shorter than 5 min were discarded to exclude events within a cluster. The histogram (bin size = 1 s) of down states 150 s before the onset of epileptic spasms was smoothed and averaged across all animals to produce spasm triggered averages. A quadratic polynomial regression model was fit to the average data to show the dependence of down state number on time. To calculate the average number of down states of the entire recording sessions, entire sessions were divided into 150-s epochs, and the number of down states was calculated and averaged across all epochs.

To analyze the production of neocortical up states prior to spasms (**Fig 5G**), candidate ictal events and preictal periods were selected with the same criteria described for down states and spasm triggered averaging was again employed. We used 2-s overlapping moving windows with 1-s steps to detect the bursts of unit activity characteristic of up states (**Fig 5G inset**). To do this, the spectral density of MUA counts (i.e. their timestamps) in the range of 1-8 Hz was computed for each window using the multitaper power spectral density estimate³⁸. In our application, spectral analysis of MUA revealed the rhythmicity of neuronal burst firing, where each rhythmic

Accepted Article

cluster of spikes is an up state (**Fig 5G inset**, in this case the peak spectral density and the up-state rhythmicity occur at 3 Hz). For a window to contain up states, the maximum MUA spectral density between 1-8 Hz had to exceed threshold, which was set at half of the peak spectral estimates of typical up-and-down-state MUA defined by binned MUA counts. The threshold was kept constant for each animal. Windows with detected up states were given a value of 1 or otherwise 0. The number of preictal time windows with detected up states was then averaged across all spasms in each animal, which yielded the proportion or probability of each 1-s step prior to the spasm containing up states. These results were smoothed and averaged across all animals. The spasm-averaged spectrogram of MUA data (**Fig 5H**) was computed using the multitaper method³⁸.

Spike Data Clustering

The first three principal components of the spike waveforms were input into the Neuralynx SpikeSort 3D program using KlustaKwik algorithm for unit clustering. A moderate isolation distance >5 were used to separate potential multiunit clusters³⁹. Units were classified as putative pyramidal units or interneurons according to their peak to trough distance, with <0.23 ms classified as putative interneurons³⁹.

HFO Analysis

HFOs during slow waves were acquired by the Neuralynx Cheetah software and manually identified with at least four oscillations clearly standing out from the background⁴⁰. Because the

HFOs analyzed were associated with the slow oscillations during NREM sleep, any contamination from electromyograph activity was highly unlikely. Moreover, by directly comparing HFO recordings to the raw LFP signals, we were able to ensure that they were not produced by electromyograph activity (large-amplitude activity over multiple electrodes in raw signals)⁴¹ or by filtering higher frequency LFP spike activity (with width <15 ms)⁴². To compute the power of the HFOs, raw signals of the slow waves were down-sampled to 3000 Hz, and the time-frequency spectrogram was computed through the complex Morlet wavelet transform. The spectral estimates were averaged across the desired frequencies (80-200 Hz for ripples and 200-500 Hz for fast ripples). The same methods used in MUA analysis were used to determine the distribution of HFOs with regards to the phase of LFP oscillations. HFO power was normalized to its maximum.

Designer Receptor Exclusively Activated by Designer Drugs (DREADD) Experiments

Viral injection. Adeno-associated virus AAV8-CamKIIa-hM3D(Gq)-mCherry was purchased from Addgene at a concentration of 1.8×10^{13} GC/ml. For control experiments, AAV8-CamKIIa-mCherry was purchased from Vector Biolabs at a titer of 2.8×10^{13} GC/ml. Viral injection was done at P25-30. A small incision (1.0 cm) was made along the incision line made previously to implant the TTX cannula. A craniotomy of 2 mm in diameter was made at the planned injection site (contralateral to the TTX cannula; -2 mm AP, -2.5 mm ML) with a sterilized 0.3-mm diameter round burr on a high-speed rotary micromotor. This allowed the injection glass micropipette (tip size, 50- μ m outer diameter and 25- μ m inner diameter) to penetrate the dura. A

total of 400 nL of virus solution was injected at the speed of 100 nL/min with a microinjection syringe pump and a SMARTouch controller (World Precision Instruments).

Surgery and drug treatments. Once the animals reached 39 to 50 days of age, an incision was made along the previous incision, the TTX cannula was removed and the rats were implanted with six 50.8 μm -diameter PFA-coated tungsten electrodes in the same cortical areas as in the thalamus experiment (**Fig 3A**). Three consecutive days of baseline video-EEG recordings were made (nine hours a day) and spasm counts were obtained by analysis of recordings. On each day of baseline recordings, rats received an injection of the clozapine vehicle (dimethylsulfoxide) immediately prior to recording. On recording day 4, rats were treated with a single dose of clozapine (1 mg/kg intraperitoneally; Selleck Chemicals), the drug that activates the receptor expressed by the transfected neocortical nerve cells. Two control groups were used. The first were animals lacking DREADD and the second were rats not treated with clozapine but with its vehicle for four days. The latter group controlled for any lingering effects of anesthesia or the surgical procedures on spasm counts.

Neurophysiological data processing. The number of spasms in clusters (**Fig 6J**) was defined as the number of spasms with inter-spasm intervals ≤ 5 min. To compute the spasm-triggered average oscillations (**Fig 7B,C**), candidate preictal periods were selected with the same methods as in MUA analysis, and LFP oscillation events were detected by using the fast-Fourier transform with Hanning windows of 1-s LFP segments in the range 1-8 Hz. The 1-s window was moved along the trace in 0.5-s steps. A threshold was set at half of the peak spectral estimates of

Accepted Article

typical interictal LFP oscillations for each animal, which could clearly separate the featured frequency from background noises. The oscillations were defined as periods where the peak spectral estimates between 1-8 Hz exceeded the threshold⁴³. Thresholds were kept constant within each animal. Windows with detected LFP oscillation events were given a value of 1 or otherwise 0. The number of windows with oscillations was counted in 3-s bins for each animal, smoothed, and averaged across all animals. For regression modeling (**Fig 7C**), the average oscillations after vehicle and clozapine treatments were catenated and modeled as a dependent variable by a quadratic polynomial predictor variable *Time* and a second variable *Drug*, where *Drug* was either 1 (clozapine) or 0 (vehicle).

All data were analyzed using a combination of freely available online MATLAB toolboxes (wICA, <http://www.mat.ucm.es/~vmakarov/downloads.php>³⁵; Chronux, <http://chronux.org>³⁸), and custom codes written in our laboratory running under MATLAB R2018b (MathWorks).

Immunohistochemistry

For immunostaining, rats were perfused with 4% paraformaldehyde, and coronal sections of the brain (100 μ m) were obtained. Mouse antibody against neurofilament (SMI32, 1:1000, BioLegend) was used to label pyramidal cells⁴⁴, and mouse antibody against parvalbumin (PV, 1:1000, Sigma-Aldrich) or rabbit antibody against PV (1:1000, Abcam) was used to identify the PV interneurons. Guinea pig antibody against vesicular glutamate transporter 2 (VGlut2, 1:1000, Millipore) was used to identify cortical layers. Confocal images were acquired with a Zeiss

880/Airyscan system. At least 12 sections were examined per rat and the two sections with the highest levels of AAV expression were imaged.

Subjects with Infantile Spasms LFP Data Processing

Analysis of clinical EEG recordings was approved by the Institutional Review Board at Baylor College of Medicine. Long-term EEG recordings were obtained from four patients with diagnosis of infantile spasms, and the EEG was recorded using the standard 10-20 international electrode placement system with a sampling rate of 256-512 Hz (Natus NicoletOne EEG system). Reference electrodes were put on the mastoid processes and the ground electrode was put at midline. The input signals were inverted. As no experimental manipulation was done, there was no randomization. The ictal events were identified by the pediatric epileptologist, and spasms within a cluster were excluded with the same criteria used in the animal model. The spasm-triggered average EEG oscillations were computed using the same methods as in animal experiments, counted in 3-s bins and averaged across all channels and ictal events. To calculate the average oscillations for entire EEG recording sessions, the EEG sessions were divided into 150-s epochs, and the number of oscillations was counted in 3-s bins and averaged across all epochs. Thresholds to detect the EEG oscillations were kept constant within each patient. The spectrogram was generated using complex Morlet wavelet transform.

Statistics

Statistical analysis was performed using custom MATLAB codes. Data were summarized as mean \pm standard errors of the mean (s.e.m.). Most of the statistical analyses in this paper used nonparametric methods, and therefore no assumption of data normality was made. Two-sided Wilcoxon rank sum test was used in the following: **Fig 2D** - unit firing rate: infragranular versus supragranular layers, **Fig 2E** – increase in unit firing: infragranular versus supragranular layers, **Fig 3D** – time of the first spike: cortex versus thalamus, **Fig 4E** – duration of interictal down state versus preictal pause, **Fig 5C** right - number of MUA spikes: epileptic versus control rats, and **Fig 5D** right – HFO power: epileptic versus control rats.

Kruskal-Wallis test followed by post hoc Wilcoxon rank sum test with Bonferroni correction was used in **Fig 2F** to compare unit firing rate during interictal, preictal pause, and ictal events. Friedman test was used followed by post hoc Wilcoxon signed rank test with Bonferroni correction in **Fig 4F** to compare interneuron and pyramidal cell firing rates across different brain states. The only parametric test used was two-sided paired-sample *t*-test to compare before-and-after-treatment differences in the same subjects. This included spasm counts and clustering: day 1-3 versus day 4 in **Fig 6I,J**, and time with oscillations: vehicle versus clozapine in **Fig 7A**. Shapiro-Wilk test was used to assess normality of data in cases where parametric tests were used. In **Fig 5C,D**, where the firing probability and HFO power in epileptic versus control rats were compared we used a two-sample Kolmogorov-Smirnov test. Quadratic regression models with time and/or drugs as predictor variables were generated to show the time and/or drug-dependence of the data in **Fig 5F,G, 7C** and **8C**. The null hypothesis is coefficient estimates of

Accepted Article

predictor variables equal to zeros, which means no relationship between predictor variables and the data. Significance level was $P < 0.05$.

Results

The Initiating Slow Wave of the Ictal Events of Epileptic Spasms Originates in Infragranular Cortical Layers

In the TTX model as in humans, the ictal complex of neocortical LFP recordings consists of an initial high-amplitude slow wave, followed by an electrodecrement. Filtering the raw signals with band-pass filters of 80-500 Hz and 600-9000 Hz yields recordings of HFOs and MUA respectively that are imbedded in the ictal event (**Fig 1A-D**). Since our previous work showed that the onset of ictal events were most often recorded contralateral to the TTX infusion site⁴⁵, we implanted a 16-channel silicon microarray into the somatosensory cortex contralateral to the TTX infusion site (**Fig 1E**). CSD analyses of the initiating slow wave were undertaken to determine: 1) if neocortical circuits were involved in the generation of the slow wave of ictal events of spasms and 2) if they were where in the laminae they were produced. We used an ICA algorithm to isolate the slow wave from other incidental events and undertook CSD analysis of the resulting LFPs³⁵. The results of CSD analysis routinely showed large current sinks in neocortical layer V and VI (**Fig 2A,B**). These results have led us to conclude that local circuits in these infragranular layers actively participate in the generation of the initiating slow wave of ictal

Accepted Article

events. Consistent with this observation were simultaneous recordings of MUA that showed much higher unit activity in the infragranular than in the supragranular cortical layers at ictal onsets (**Fig 2C-E**, 255.5 ± 23.9 versus 69.9 ± 10.9 Hz, $P = 6.5 \times 10^{-10}$). Moreover, **Fig 2E-inset** indicates that at ictal onset, unit firing in infragranular layers preceded that of supragranular layers. During the initial 10 ms of ictal events, infragranular unit firing greatly exceeded that of supragranular neurons ($334 \pm 39\%$ versus $161 \pm 48\%$, $P = 6.3 \times 10^{-9}$, Wilcoxon rank sum test, $n = 55$ ictal events) when normalized to interictal baseline firing rates. Well known excitatory synaptic projections from layer V pyramidal cells to layer II/III neurons⁴⁶⁻⁴⁸ could explain this difference in timing.

One long-standing question has been the contributions of cortical and subcortical circuits to the generation of spasms. In several models of epilepsy, interactions between the cortex and thalamocortical projections from the ventrobasal complex have been implicated in seizure generation^{49, 50}. To begin to address this issue, we implanted tungsten wires bilaterally into ventrobasal complex of the thalamus and simultaneously recorded ictal events from six sites in cortex (**Fig 3A,B**). Consistent with the neocortex initiating the generation of spasms, we found neocortical cells always fired before the thalamic ventrobasal complex cells at ictal onset (66.9 ms earlier, **Fig 3C,D**, $P = 6.1 \times 10^{-15}$). Taken together, results of both CSD and MUA analyses suggest that neocortical networks in infragranular layers likely initiate the generation of ictal events.

An Unexpected Pause in MUA Prior to the Ictal Onset Shares Features with Neocortical Interictal Down States

When examining MUA at the onset of ictal events, we observed a dramatic pause in unit activity immediately prior to ictal events (**Fig 2C,E**). Quantitatively, we detected an 82% decrease in unit firing rate during the preictal pause compared to interictal baseline (**Fig 2F**, 9.6 ± 2.9 versus 52.8 ± 10.6 Hz, $P = 5.7 \times 10^{-6}$). Before 72% (36/50) of ictal events, unit activity ceased and in the remaining 28% a reduction in MUA was recorded. Our initial impression was that these pauses in neuronal activity resembled the neocortical down states of NREM sleep. Since our recordings were made during daytime and rats are nocturnal animals, 90% (103/115) of spasms were recorded during sleep or transitioning between it and waking. This provided an opportunity to study the interplay between the operations of neocortical networks during sleep and the generation of epileptic spasms. To explore the possibility that the preictal pause was in some way related to neocortical down states, we compared the MUA during interictal down states to that of the pause. In addition, we sorted units into putative interneurons and pyramidal units to determine whether different neurons behaved the same or differently during these two periods. Although spike sorting during seizures can be difficult, studies have shown it can be achieved^{39,51}. We found that putative interneuron single units could be well isolated, but during seizures the putative pyramidal unit activity was most likely produced by several pyramidal cells (**Fig 4C**). **Fig 4A** shows a slow time base LFP recording comparing an ictal event (arrow) and a series of rhythmic interictal slow wave oscillations (for clarity arrow heads denote three of these

slow waves), and the raster plots illustrate the marked rhythmic changes in unit firing that were coincident with the oscillations in LFP recordings. **Fig 4B** compares raster plots of the ictal event and one cycle of the interictal oscillations at a faster time base and illustrates the dramatic transition from the apparent down states to up states for both events. From such recordings, we first compared the duration of interictal down states to that of the preictal pause. Histograms in **Fig 4D** showed the temporal patterning of MUA in the two states to be very similar and an analysis of their durations showed they were essentially the same (**Fig 4E**). Next, we found that putative interneuron firing was abolished during both the preictal pause and interictal down state (**Fig 4F**). Similarly, most pyramidal cells were silent during both periods (**Fig 4B**), however, a minority of them remained active. This resulted in the average putative pyramidal cell activity being low but was of equal intensity during these two periods (**Fig 4F**). Finally, and remarkably, unit firing ceased across the cortical laminae during both the pause (**Fig 2C**) and interictal down states (**Fig 5A**). Taken together, these results suggest that the preictal pause shares many features with interictal down states.

Comparison of the Ictal Events of Epileptic Spasms to Interictal Up States

Given that our results suggest that the preictal pause could be an interictal down state, it follows that the subsequent ictal event of epileptic spasms may be produced by an ensuing but unusually intense up state. To explore this possibility, we compared unit spiking during interictal up states to that during ictal events. **Fig 4D** shows that firing rates during ictal events were much greater than during up states. However, for putative interneurons, firing rates during interictal up

Accepted Article

states were essentially identical to those during ictal events, while putative pyramidal unit firing rate was significantly higher during the ictal discharge than the interictal up state (**Fig 4F**, 213.3 ± 13.5 versus 100.4 ± 9.2 Hz, $P = 4.7 \times 10^{-15}$). The firing pattern of putative interneurons and putative pyramidal units were similar. During the interictal period, both putative interneurons and pyramidal units firing were clustered at the peak of the slow wave oscillations. At the onset of ictal events, there was a surge of firing for both putative interneurons and pyramidal units after the pause (**Fig 4G**).

Given the proposition that the ictal events of spasms may be produced by an unusually intense up state, we wondered if there were differences in the operation of neocortical networks in epileptic animals during NREM sleep that could predispose the cortex to generate more intense up states and consequently ictal events. We suspected major differences existed since the LFP spectrogram during NREM sleep showed very intense spectral peaks below 8 Hz in epileptic animals and while controls displayed a similar range of low frequencies these were less uniform and of much lower power (**Fig 5B**). Given these differences, we compared LFP and MUA during NREM sleep in epileptic and control rats and found the MUA firing patterns were very different between the two groups (**Fig 5A**). The firing probability in epileptic animals was sharply peaked for the interictal oscillations while the control distribution was more widely distributed (**Fig 5C**, left). The number of spikes was also significantly larger at the peak of LFP oscillations (0 radian) in epileptic rats (**Fig 5C**, right, 8.3 ± 0.6 versus 4.4 ± 0.5 , $P = 1.1 \times 10^{-16}$). Consistent with these findings were an analysis of simultaneously recorded HFO activity. Like MUA, HFO power in

the fast ripple frequency (200-500 Hz) was largest and clustered at the peak of interictal oscillations in epileptic animals but was widely distributed across the slow waves in controls (**Fig 5D**, left). Moreover, fast ripple power was significantly larger at the peak of the interictal oscillations in epileptic animals (**Fig 5D**, right, 995.2 ± 261.8 versus $373.0 \pm 48.5 \mu\text{V}^2/\text{Hz}$, $P = 0.011$). Taken together, results suggest that the interictal up states in epileptic rats are unusually intense and this raises the possibility that they could occasionally produce ictal events.

If the interictal down to up state transitions play a role in spasm generation during NREM sleep, then it would follow that an analysis of up and down states prior to spasms could reveal a correlation in time between the occurrence of spasms and frequency of up-and-down-state sequences. Recordings and the spectrogram in **Fig 5E** indicate that this might be the case. Here an animal's sleep states transitioned from NREM (where up-and-down-state sequences occur) to REM and back to NREM again immediately before ictal onset. To explore the potential relationships between up-and-down-state sequences and ictal events, we used spasm-triggered averaging and quantified up-and-down-state sequences through analysis of MUA several minutes prior to the onset of ictal events. Two methods were used: we calculated the number of down states and probability of up states. When we analyzed the preictal periods across four animals with 63 ictal events we found an increase in the number of down states as recordings approached the onset of ictal events. This could be modeled by a quadratic polynomial regression model (red line) with time to spasms as the predictor variable (**Fig 5F**). In contrast, when succeeding 150-s epochs of entire recordings sessions (>4 hours) were analyzed no variations in down state

number were observed (**Fig 5F, inset**). We also analyzed the probability of cortical networks having up states by spectral analysis of MUA counts (see Materials and Methods) and found a similar pattern of an increase in up state probability immediately prior to the onset of ictal events (**Fig 5G**). The spectrogram (**Fig 5H**) of MUA further exemplifies the trough and ramp-up in up states prior to spasms. These results suggest that a ramp-up in the number of up-and-down-state sequences per unit time just prior to spasms may predispose cortical networks to initiate ictal events.

Chemogenetic Activation of Neocortical Pyramidal Cells Increases Spasm Counts and Spasm Clustering

Results in **Fig 2** suggest that infragranular neocortical networks contribute to the generation of ictal events and **Fig 5** suggests that unusually large and frequent neocortical up states likely play a role in initiating the ictal events of spasms. Previous studies have shown that during up states neocortical neurons simultaneously receive balanced barrages of recurrent excitatory and inhibitory synaptic potentials^{30, 31, 52}. Based on what appears to be increased up state intensity in epileptic rats (**Fig 5**), we hypothesized that the selective activation of neocortical pyramidal cells in epileptic animals might shift the excitation/inhibition balance favoring excitation and this could increase the frequency of spasms – although alternative outcomes were possible (see Discussion). To address our hypothesis, we used the designer receptor exclusively activated by designer drugs (DREADD) technique to selectively activate neocortical pyramidal cells. We injected AAV8-CamKIIa-hM3D(Gq)-mCherry into infragranular layers of the left

somatosensory cortex (**Fig 6A**). Immunohistochemical results and confocal imaging showed that pyramidal cells were transfected by the virus, but parvalbumin interneurons did not express the viral reporter, mCherry (**Fig 6B**). It has been reported that DREADD receptor activation by the often-used designer drug clozapine-N-oxide (CNO) occurs once it is metabolized to clozapine⁵³. Accordingly, we used clozapine as the ligand to activate the DREADD receptors. In pilot experiments, we treated rats with clozapine dosage at 0.05, 0.1, 0.5, 1.0, 5.0, and 10.0 mg/kg (total $n = 12$). Epileptic animals with DREADD receptors showed no response to dosages below 1.0 mg/kg but appeared to respond to 1.0 mg/kg with an increase in spasm counts. However, at 5.0 mg/kg, the animals appeared drowsy and at 10.0 mg/kg animals were sedated and the interictal LFP oscillations were suppressed. Thus, we chose the 1.0 mg/kg dosage for experiments.

We used several control groups to rule out off-target drug effects. In the first, three naïve control rats were transfected with the virus and treated with clozapine. These rats never displayed epileptic spasms, however within two hours of treatment all developed focal epileptiform activity and two displayed subclinical focal seizures that were initiated at the virus injection site (**Fig 6C**) – a result expected if clozapine acts primarily to increase the activity of virally transfected pyramidal cells⁵⁴.

In terms of epileptic rats, one control group (Epi-No DREADD) consisted of five animals with spasms that either did not receive a viral injection ($n = 2$) or were injected with virus without hM3D(Gq) receptors (AAV8-CamKIIa-mCherry) ($n = 3$). Another control group consisted of

Accepted Article

five animals with DREADD but were not treated with clozapine; instead these controls received the vehicle for four days (Epi-No CLZ). In both epileptic control groups, we observed no change in spasm counts whether they lacked DREADD (**Fig 6F,I**) or were not treated with clozapine (**Fig 6G,I**). In sharp contrast, our experimental group, which consisted of epileptic animals injected with the hM3D(Gq)-containing virus (Epi-DREADD+CLZ), had a 1.73 fold increase in spasm counts (**Fig 6H,I**, 39.3 ± 5.2 versus 22.7 ± 3.9 , $P = 0.012$) and a 3.47 fold increase in spasm clustering (**Fig 6H,J**, 22.2 ± 5.5 versus 6.4 ± 2.4 , $P = 0.025$) following clozapine treatment. The ictal events recorded after clozapine treatment (**Fig 6E**) in epileptic rats had the same electrophysiologic and behavioral features as the spontaneous spasms observed during baseline recordings (**Fig 6D**) and were in sharp contrast to the focal seizures induced in non-epileptic controls (**Fig 6C**). In short, chemogenetic results support the hypothesis that epileptic spasms can be produced by neocortical pyramidal cell activity and spasms can arise from neocortical networks.

Chemogenetic Activation of Neocortical Pyramidal Cells Also Increases Interictal Slow Wave Oscillations Prior to Spasms

Since activating neocortical pyramidal cells increases spasm counts and other results implicate up states in the initiation of spasms, we examined the possibility that clozapine treatment might increase the number of interictal slow wave oscillations. Typically, these oscillations are below 8 Hz. Thus, we first calculated the percent time that networks oscillated at 1-8 Hz in the two hours after clozapine treatment. Activating neocortical pyramidal cells significantly increased the time

LFP oscillated at these frequencies in the DREADD transfected group (**Fig 7A**, $47 \pm 11\%$ versus $36 \pm 11\%$, $P = 0.0047$) but not in their epileptic controls that did not express DREADD ($P = 0.15$).

We next examined spasm-triggered average oscillations in the preictal periods and observed a ramp-up in the number of oscillations just prior to the onset of ictal events (**Fig 7B**). This recapitulated the results from the MUA analysis (**Fig 5F,G**). The graphs and spectrograms in **Fig 7C,D** show that after clozapine treatment, we still observed an increase in LFP oscillations just prior to ictal events but the number of oscillations was higher. By using a quadratic polynomial regression model we could relate the number of oscillations to both time to spasm and drug treatment (vehicle or clozapine) (**Fig 7C**). Thus, results suggest that DREADD activation of neocortical pyramidal cells increases the number of LFP oscillations and hence the cortical up-and-down-state sequences immediately prior to ictal events. This could be one mechanism by which DREADD-induced increases in pyramidal cell activity influence the generation of spasms.

The Number of Slow Wave Oscillations Increases during Preictal Periods in Infantile Spasms Patients

Since we observed an increase in number of cortical up and down states prior to the onset of ictal events in an animal model (**Fig 5F and 7B**), we then asked whether we could observe a similar phenomenon in patients with infantile spasms. We analyzed all channels ($n = 19$, standard 10/20 electrode placement) of long-term (6-12 hours) EEG recordings from four patients in the epilepsy monitoring unit using the same methods as described for the animals. We found an

Accepted Article

increase in the number of LFP oscillations during preictal periods similar to the findings in the TTX model (**Fig 8A,B**), and a U-shaped spasm-triggered average plot and the spectrogram for EEG oscillations with a trough at 50-100 s before the onset of epileptic spasms (**Fig 8C,D**). By comparison, analysis of 150-s epochs from the entire recording sessions failed to show any variations in the occurrence of slow oscillations (**Fig 8E**).

Discussion

We focused our efforts on exploring the possibility that spasm generation is initiated in the cortex in the TTX animal model. The results from CSD and MUA analyses implicated neuronal circuits in the infragranular layers in generating the initiating slow wave of ictal events. Unexpectedly, we routinely observed a pause or reduction in unit firing immediately before the onset of spasms and provide evidence that these pauses share features with the interictal neocortical down states of NREM sleep. Additional analyses suggested subsequent ictal events were likely produced by an ensuing very large up state, which further supported a role for the cortex in spasm generation. Our observation that chemogenetic activation of neocortical pyramidal cell in epileptic rats increased the occurrence of spasms further bolstered arguments supporting a neocortical-initiating hypothesis. We also observed an increase in the number of up-and-down-state oscillations in the minutes preceding ictal events which provided additional evidence for an unappreciated interplay between brain state mechanisms and spasm generation.

Results from CSD analysis revealed current sinks in cortical layer V and VI laminae that have been shown previously to be most able to generate epileptiform activity and seizures in numerous models^{46, 55-57}. The propensity of these layers to produce seizures is thought to be due to the presence of dense pyramidal cell recurrent excitatory networks. An interesting parallel is that normal slow waves are predominantly generated in deep cortical layers^{30, 58}. Moreover, recent reexamination of clinical EEG data and *in vitro* slice results have led to computer models that implicate layer V pyramidal cells in the generation of epileptic spasms^{59, 60}. Our analysis of MUA also shows robust activity in the deep cortical layers at ictal onset that precedes unit activity in more superficial layers. These results are consistent with the idea that recurrent excitatory networks located infragranularly initiate ictal events but activity can quickly spread supragranularly through local excitatory synaptic pathways⁴⁶⁻⁴⁸.

The existence of a pause in neuronal activity preceding spasms was unexpected. We identified four features of preictal pauses in Results that match those of interictal network down states. Since the preictal pause shares many features with network down states, it follows that the subsequent ictal event may be the product of an ensuing but unusually large up state. Our observations that MUA and HFO power are more focused and intense at the peak of LFP oscillations in epileptic rats compared to controls support the idea that interictal up states are more intense in epileptic animals. We also found putative pyramidal cell firing rates were much higher during ictal events than interictal up states. However, interneuron firing was very similar

between the two states - pointing to a potential imbalance in excitation and inhibition that could contribute to the generation of ictal events.

Since our multielectrode array recordings pointed to neuronal circuits in layers V and VI as contributors to the generation of spasms, we reasoned that experimental interventions that increase the excitability of pyramidal cells in these laminae should increase the frequency of spasms. To test this hypothesis, we used a DREADD technique that allowed us to predominantly activate infragranular pyramidal cells. Our results show that activation of the DREADD with clozapine did indeed increase spasm counts and clustering. An alternative outcome would have been that the activation of pyramidal cells produced a persistent network up state which would result in the elimination of slow wave oscillations. However, this was not observed, and one reason could be that not every pyramidal cell in the relatively small targeted region of cortex was transfected. This could allow slow wave oscillations to persist and up state intensity to be enhanced due to the increased excitability of those pyramidal cells that were transfected.

Our analyses of MUA and LFPs showed a gradual increase in oscillatory activity towards the onset of ictal events. This suggests that an increase in number of up-and-down-state sequences can influence spasm generation. A similar trend was observed in human patients. Activation of cortical layer V pyramidal cells have been shown to be sufficient to initiate up states^{30, 61, 62}, and in the TTX model activation of infragranular pyramidal cells increased the frequency of interictal oscillations (**Fig 7A,C,D**). This could be one contributing mechanism by which pyramidal cell

Accepted Article

activation increases spasm number and clustering. However, our analysis suggests that not every spasm is preceded by a ramp-up in slow wave oscillations – an increase in oscillations may simply increase the likelihood that the concurrent up states will produce a spasm. At other times, an isolated intense up state or other mechanism(s) may produce a spasm in the absence of preceding oscillations.

Experiments reported here were focused on advancing an understanding of the mechanisms underlying the ictal event of epileptic spasms. Clinically, the slow wave/electrodecrement ictal complex of spasms has been recorded in infants, older children, adolescents and adults^{2-4, 7-11, 63}. Thus, our findings should have implications for future studies in all these age groups. Nonetheless, it is worth considering the epileptic spasm patient population the TTX animal model most closely resembles. In our experiments, spasms are induced by chronic infusion of TTX beginning on P10-12⁶⁴. Spasms cannot be induced by TTX in older animals⁶⁵. Thus, the induction is developmentally dependent. In addition, an earlier study showed that TTX induces a neocortical lesion at its infusion site which recapitulates the early-life brain injury etiologies for infantile spasms²⁴. While the similarities and differences between human and rodent brain development have been debated for decades, many believe P7-10 are comparable to a term human infant⁶⁶. Given this, spasms in the TTX model are likely induced at a time comparable to the neonatal period in humans. Behavioral spasms first appear a week later which is thought to be a time comparable to human infancy⁶⁷. This delay in the onset of spasms is reminiscent of the delay between brain injuries in humans (e.g. perinatal stroke) and the first occurrence of

Accepted Article

spasms⁶⁸. Perhaps most notably, epileptic spasms in the TTX model persist for at least 2-3 months, but this is also not unlike what is observed in some patients. While epileptic spasms are most frequent during infancy in humans, they have been reported to persist in up to 16 and 19% of patients beyond age of 3 and 7 respectively^{5, 6}. They have been well documented in adolescents and adults (all former infantile spasm patients) with the same electrophysiological and behavioral features^{2, 4}. One study focused on patients that were successfully treated as infants, but epileptic spasms recurred up to six years later and were described as “identical to the initial spasms”³. Thus, given the age of spasm induction and onset and their endurance, the spasms studied in experiments reported here are likely to most closely resemble epileptic spasms that persist beyond infancy.

Studies reported here examined epileptogenic mechanisms contralateral to the TTX lesion. This experimental strategy was based on our previous study that reported that spasms most often arise contralaterally⁴⁵. However, those results also showed that ictal events can also arise ipsilateral to the lesion. We do not contend that the contralateral cortex is the only cortical region capable of generating spasms but just one region with this potential. Finally, our results do not preclude subcortical areas from also participating in the production of behavioral spasms. It is possible that other brain areas intercede between the cortex and spinal motor neurons and contribute to behavioral spasm generation.

Acknowledgements

This work was funded by CURE's Infantile Spasms Initiative and NIH NINDS grants: RO1 NS018309 and RO1 NS105913 to J.W.S. It was also supported by IDDRC grant 1U54 HD083092 from the Eunice Kennedy Shriver National Institute of Child Health & Human Development. The authors would like to acknowledge Dr. Dinghui Yu and the IDDRC Microscopy Core at the NRI; we would also like to thank Dr. Mingshan Xue for advice and discussions on AAV transfections and Dr. Matt McGinley for valuable input on an early draft of this paper. We also acknowledge Trang Lam for excellent technical assistance.

Author Contributions

C.-H.L. and J.W.S. contributed to the conception and design of the study; C.-H.L., J.T.L., C.J.B.-R., and A.E.A. contributed to the acquisition and analysis of data; C.-H.L. and J.W.S. contributed to drafting the text and preparing the figures.

Potential Conflicts of Interest

Nothing to report.

References

- Accepted Article
1. Pellock JM, Hrachovy R, Shinnar S, et al. Infantile spasms: a U.S. consensus report. *Epilepsia*. 2010 Oct;51(10):2175-89.
 2. de Menezes MA, Rho JM. Clinical and electrographic features of epileptic spasms persisting beyond the second year of life. *Epilepsia*. 2002 Jun;43(6):623-30.
 3. Camfield P, Camfield C, Lortie A, Darwish H. Infantile spasms in remission may reemerge as intractable epileptic spasms. *Epilepsia*. 2003 Dec;44(12):1592-5.
 4. Talwar D, Baldwin MA, Hutzler R, Griesemer DA. Epileptic spasms in older children: persistence beyond infancy. *Epilepsia*. 1995 Feb;36(2):151-5.
 5. Riikonen R. A long-term follow-up study of 214 children with the syndrome of infantile spasms. *Neuropediatrics*. 1982 2/1982;13(1):14-23.
 6. Jeavons PM, Bower BD, Dimitrakoudi M. Long-term prognosis of 150 cases of "West syndrome". *Epilepsia*. 1973 Jun;14(2):153-64.
 7. Ronzano N, Valvo G, Ferrari AR, Guerrini R, Sicca F. Late-onset epileptic spasms: clinical evidence and outcome in 34 patients. *J Child Neurol*. 2015 Feb;30(2):153-9.
 8. Eisemann MM, Ville D, Soufflet C, et al. Cryptogenic late-onset epileptic spasms: an overlooked syndrome of early childhood? *Epilepsia*. 2006 Jun;47(6):1035-42.
 9. Auvin S, Lamblin MD, Pandit F, Vallee L, Bouvet-Mourcia A. Infantile epileptic encephalopathy with late-onset spasms: report of 19 patients. *Epilepsia*. 2010 Jul;51(7):1290-6.
 10. Cerullo A, Marini C, Carcangiu R, Baruzzi A, Tinuper P. Clinical and video-polygraphic features of epileptic spasms in adults with cortical migration disorder. *Epileptic Disord*. 1999 Mar;1(1):27-33.
 11. Hrachovy RA. West's syndrome (infantile spasms). Clinical description and diagnosis. *AdvExpMedBiol*. 2002 2002;497:33-50.
 12. Chugani HT, Shewmon DA, Sankar R, Chen BC, Phelps ME. Infantile spasms: II. Lenticular nuclei and brain stem activation on positron emission tomography. *AnnNeurol*. 1992 2/1992;31(2):212-9.
 13. Hrachovy RA, Frost JD, Jr., Kellaway P. Sleep characteristics in infantile spasms. *Neurology*. 1981 6/1981;31(6):688-93.
 14. Avanzini G, Panzica F, Franceschetti S. Brain maturational aspects relevant to pathophysiology of infantile spasms. *Int Rev Neurobiol*. 2002;49:353-65.
 15. Chugani HT, Shields WD, Shewmon DA, Olson DM, Phelps ME, Peacock WJ. Infantile spasms: I. PET identifies focal cortical dysgenesis in cryptogenic cases for surgical treatment. *AnnNeurol*. 1990 4/1990;27(4):406-13.
 16. Chugani HT, Shewmon DA, Shields WD, et al. Surgery for intractable infantile spasms: neuroimaging perspectives. *Epilepsia*. 1993 Jul-Aug;34(4):764-71.
 17. Iwatani Y, Kagitani-Shimono K, Tominaga K, et al. Long-term developmental outcome in patients with West syndrome after epilepsy surgery. *Brain Dev*. 2012 Oct;34(9):731-8.
 18. Kang JW, Rhie SK, Yu R, et al. Seizure outcome of infantile spasms with focal cortical dysplasia. *Brain Dev*. 2013 Sep;35(8):816-20.
 19. Chugani HT, Ilyas M, Kumar A, et al. Surgical treatment for refractory epileptic spasms: The Detroit series. *Epilepsia*. 2015 Dec;56(12):1941-9.
 20. Chugani HT. Pathophysiology of infantile spasms. *Adv Exp Med Biol*. 2002;497:111-21.
 21. Frost JD, Jr., Lee CL, Le JT, Hrachovy RA, Swann JW. Interictal high frequency oscillations in an animal model of infantile spasms. *Neurobiol Dis*. 2012 May;46(2):377-88.

22. Bragin A, Engel J, Jr., Wilson CL, Fried I, Mathern GW. Hippocampal and entorhinal cortex high-frequency oscillations (100–500 Hz) in human epileptic brain and in kainic acid–treated rats with chronic seizures. *Epilepsia*. 1999 Feb;40(2):127-37.
23. Bragin A, Engel J, Jr., Wilson CL, Fried I, Buzsaki G. High-frequency oscillations in human brain. *Hippocampus*. 1999;9(2):137-42.
24. Frost JD, Jr., Le JT, Lee CL, Ballester-Rosado C, Hrachovy RA, Swann JW. Vigabatrin therapy implicates neocortical high frequency oscillations in an animal model of infantile spasms. *Neurobiol Dis*. 2015 Oct;82:1-11.
25. Steriade M, Nunez A, Amzica F. A novel slow (< 1 Hz) oscillation of neocortical neurons in vivo: depolarizing and hyperpolarizing components. *J Neurosci*. 1993 Aug;13(8):3252-65.
26. Steriade M, Nunez A, Amzica F. Intracellular analysis of relations between the slow (< 1 Hz) neocortical oscillation and other sleep rhythms of the electroencephalogram. *J Neurosci*. 1993 Aug;13(8):3266-83.
27. Steriade M, Contreras D, Curro Dossi R, Nunez A. The slow (< 1 Hz) oscillation in reticular thalamic and thalamocortical neurons: scenario of sleep rhythm generation in interacting thalamic and neocortical networks. *J Neurosci*. 1993 Aug;13(8):3284-99.
28. Timofeev I, Grenier F, Steriade M. Disfacilitation and active inhibition in the neocortex during the natural sleep-wake cycle: an intracellular study. *Proc Natl Acad Sci U S A*. 2001 Feb 13;98(4):1924-9.
29. Petersen CC, Hahn TT, Mehta M, Grinvald A, Sakmann B. Interaction of sensory responses with spontaneous depolarization in layer 2/3 barrel cortex. *Proc Natl Acad Sci U S A*. 2003 Nov 11;100(23):13638-43.
30. Sanchez-Vives MV, McCormick DA. Cellular and network mechanisms of rhythmic recurrent activity in neocortex. *Nat Neurosci*. 2000 Oct;3(10):1027-34.
31. Shu Y, Hasenstaub A, McCormick DA. Turning on and off recurrent balanced cortical activity. *Nature*. 2003 May 15;423(6937):288-93.
32. David F, Schmiedt JT, Taylor HL, et al. Essential thalamic contribution to slow waves of natural sleep. *J Neurosci*. 2013 Dec 11;33(50):19599-610.
33. Lee CL, Frost JD, Jr., Swann JW, Hrachovy RA. A new animal model of infantile spasms with unprovoked persistent seizures. *Epilepsia*. 2008 Feb;49(2):298-307.
34. Wirrell EC, Shellhaas RA, Joshi C, et al. How should children with West syndrome be efficiently and accurately investigated? Results from the National Infantile Spasms Consortium. *Epilepsia*. 2015 Apr;56(4):617-25.
35. Fernandez-Ruiz A, Makarov VA, Benito N, Herreras O. Schaffer-specific local field potentials reflect discrete excitatory events at gamma frequency that may fire postsynaptic hippocampal CA1 units. *J Neurosci*. 2012 Apr 11;32(15):5165-76.
36. Mitzdorf U. Current source-density method and application in cat cerebral cortex: investigation of evoked potentials and EEG phenomena. *Physiol Rev*. 1985 Jan;65(1):37-100.
37. Ji D, Wilson MA. Coordinated memory replay in the visual cortex and hippocampus during sleep. *Nat Neurosci*. 2007 Jan;10(1):100-7.
38. Bokil H, Andrews P, Kulkarni JE, Mehta S, Mitra PP. Chronux: a platform for analyzing neural signals. *J Neurosci Methods*. 2010 Sep 30;192(1):146-51.

39. Neumann AR, Raedt R, Steenland HW, et al. Involvement of fast-spiking cells in ictal sequences during spontaneous seizures in rats with chronic temporal lobe epilepsy. *Brain*. 2017 Sep 1;140(9):2355-69.
40. Jacobs J, Staba R, Asano E, et al. High-frequency oscillations (HFOs) in clinical epilepsy. *Prog Neurobiol*. 2012 Sep;98(3):302-15.
41. Zijlmans M, Worrell GA, Dimpelmann M, et al. How to record high-frequency oscillations in epilepsy: A practical guideline. *Epilepsia*. 2017 Aug;58(8):1305-15.
42. Benar CG, Chauviere L, Bartolomei F, Wendling F. Pitfalls of high-pass filtering for detecting epileptic oscillations: a technical note on "false" ripples. *Clin Neurophysiol*. 2010 Mar;121(3):301-10.
43. Katznel D, Nicholson E, Schorge S, Walker MC, Kullmann DM. Chemical-genetic attenuation of focal neocortical seizures. *Nat Commun*. 2014 May 27;5:3847.
44. van der Gucht E, Vandesande F, Arckens L. Neurofilament protein: a selective marker for the architectonic parcellation of the visual cortex in adult cat brain. *J Comp Neurol*. 2001 Dec 24;441(4):345-68.
45. Frost JD, Jr., Lee CL, Hrachovy RA, Swann JW. High frequency EEG activity associated with ictal events in an animal model of infantile spasms. *Epilepsia*. 2011 Jan;52(1):53-62.
46. Connors BW. Initiation of synchronized neuronal bursting in neocortex. *Nature*. 1984 Aug 23-29;310(5979):685-7.
47. Chagnac-Amitai Y, Luhmann HJ, Prince DA. Burst generating and regular spiking layer 5 pyramidal neurons of rat neocortex have different morphological features. *J Comp Neurol*. 1990 Jun 22;296(4):598-613.
48. Larsen DD, Callaway EM. Development of layer-specific axonal arborizations in mouse primary somatosensory cortex. *J Comp Neurol*. 2006 Jan 20;494(3):398-414.
49. Paz JT, Davidson TJ, Frechette ES, et al. Closed-loop optogenetic control of thalamus as a tool for interrupting seizures after cortical injury. *Nat Neurosci*. 2013 Jan;16(1):64-70.
50. Sorokin JM, Davidson TJ, Frechette E, et al. Bidirectional Control of Generalized Epilepsy Networks via Rapid Real-Time Switching of Firing Mode. *Neuron*. 2017 Jan 4;93(1):194-210.
51. Truccolo W, Donoghue JA, Hochberg LR, et al. Single-neuron dynamics in human focal epilepsy. *Nat Neurosci*. 2011 May;14(5):635-41.
52. Tahvildari B, Wolfel M, Duque A, McCormick DA. Selective functional interactions between excitatory and inhibitory cortical neurons and differential contribution to persistent activity of the slow oscillation. *J Neurosci*. 2012 Aug 29;32(35):12165-79.
53. Gomez JL, Bonaventura J, Lesniak W, et al. Chemogenetics revealed: DREADD occupancy and activation via converted clozapine. *Science*. 2017 Aug 4;357(6350):503-7.
54. Alexander GM, Rogan SC, Abbas AI, et al. Remote control of neuronal activity in transgenic mice expressing evolved G protein-coupled receptors. *Neuron*. 2009 Jul 16;63(1):27-39.
55. Telfeian AE, Connors BW. Layer-specific pathways for the horizontal propagation of epileptiform discharges in neocortex. *Epilepsia*. 1998 Jul;39(7):700-8.
56. Jin X, Prince DA, Huguenard JR. Enhanced excitatory synaptic connectivity in layer v pyramidal neurons of chronically injured epileptogenic neocortex in rats. *J Neurosci*. 2006 May 3;26(18):4891-900.

57. Polack PO, Guillemain I, Hu E, Deransart C, Depaulis A, Charpier S. Deep layer somatosensory cortical neurons initiate spike-and-wave discharges in a genetic model of absence seizures. *J Neurosci*. 2007 Jun 13;27(24):6590-9.
58. McCormick DA, McGinley MJ, Salkoff DB. Brain state dependent activity in the cortex and thalamus. *Curr Opin Neurobiol*. 2015 Apr;31:133-40.
59. Janicot R, Shao LR, Stafstrom CE. Infantile Spasms: An Update on Pre-Clinical Models and EEG Mechanisms. *Children (Basel)*. 2020 Jan 6;7(1).
60. Traub RD, Moeller F, Rosch R, Baldeweg T, Whittington MA, Hall SP. Seizure initiation in infantile spasms vs. focal seizures: proposed common cellular mechanisms. *Rev Neurosci*. 2020 Jan 28;31(2):181-200.
61. Chauvette S, Volgushev M, Timofeev I. Origin of active states in local neocortical networks during slow sleep oscillation. *Cereb Cortex*. 2010 Nov;20(11):2660-74.
62. Beltramo R, D'Urso G, Dal Maschio M, et al. Layer-specific excitatory circuits differentially control recurrent network dynamics in the neocortex. *Nat Neurosci*. 2013 Feb;16(2):227-34.
63. Kellaway P, Hrachovy RA, Frost JD, Jr., Zion T. Precise characterization and quantification of infantile spasms. *Ann Neurol*. 1979 9/1979;6(3):214-8.
64. Lee CL, Frost Jr. JD, Swann JW, Hrachovy RA. A New Animal Model of Infantile Spasms with Unprovoked Persistent Seizures. *Epilepsia*. 2008 2008;49:298-307.
65. Galvan CD, Hrachovy RA, Smith KL, Swann JW. Blockade of neuronal activity during hippocampal development produces a chronic focal epilepsy in the rat. *J Neurosci*. 2000 2000;20(8):2904-16.
66. Semple BD, Blomgren K, Gimlin K, Ferriero DM, Noble-Haeusslein LJ. Brain development in rodents and humans: Identifying benchmarks of maturation and vulnerability to injury across species. *Prog Neurobiol*. 2013 Jul-Aug;106-107:1-16.
67. Stafstrom CE, Holmes GL. Infantile spasms: criteria for an animal model. *Int Rev Neurobiol*. 2002 2002;49:391-411.
68. Golomb MR, Garg BP, Williams LS. Outcomes of children with infantile spasms after perinatal stroke. *Pediatric neurology*. 2006 Apr;34(4):291-5.

Figure Legends

FIGURE 1: An ictal event of an epileptic spasm. (A) Ictal complex consisting of an initial large-amplitude slow wave (SW) and the following electrodecrement. With different filter settings (B) the local field potential (LFP), (C) high frequency oscillations (HFOs) (80-500 Hz), and (D) multiunit activity (MUA) (600-9000 Hz) are revealed. (E) Representative

immunohistological staining showing location of the silicon microarray (marked by DiI) implanted in the somatosensory cortex. Drawing of electrode overlays the electrode track. VGlut2 immunohistochemistry (green) was used to delineate cortical laminae.

FIGURE 2: The ictal events of epileptic spasms originate in infragranular cortical layers, with a preictal MUA pause occurring before their onset. (A) Representative result of the independent component analysis-current source density algorithm shows a current sink (warm color) at channels 13 and 14 in the infragranular layers. Time 0 marks the peak of the initial ictal slow wave. Right panel: LFP recordings of the initiating slow wave; Center: computed CSD; Left: color coded CSD. (B) Summary of CSD analyses from nine animals (10 spasms were analyzed from each rat). Only current sinks (warm color) are shown. (C) Representative CSD, LFP, and raster plot of MUA spikes during an ictal event. Preictal pause is depicted by red brackets. Time 0 is the peak of the initial ictal slow wave. (D) Comparison of MUA firing rate during the first 200 ms of ictal events between supragranular (Supra) and infragranular (Infra) layers (Wilcoxon rank sum test, $***P = 6.5 \times 10^{-10}$; $n = 55$ ictal events from five animals). (E) Average peri-ictal time histogram comparing MUA firing rate within supragranular (blue) and infragranular (red) layers. **Inset**, peri-ictal time histogram at faster time base comparing onset of MUA (bin size = 10 ms; $n = 55$ ictal events from five animals; time 0 is the first spike of MUA at ictal onset). (F) Average MUA firing rates during the interictal and ictal periods and preictal pauses (Kruskal-Wallis test followed by post hoc Wilcoxon rank sum test with Bonferroni

Accepted Article
correction, $P = 4.4 \times 10^{-21}$; interictal versus pause, $P = 5.7 \times 10^{-6}$; pause versus ictal, $P = 9.5 \times 10^{-18}$; interictal versus ictal, $P = 8.3 \times 10^{-11}$; $n = 55$ ictal events from five animals; $***P < 0.001$).

FIGURE 3: Neocortical cells fire before those of thalamic ventrobasal complex (VB) at the onset of an ictal event. (A) Locations of cortical (1-6) and VB (7-8) recording electrodes and the TTX infusion site. Gnd, ground electrode; Ref, reference electrode. (B) Immunohistological staining showing the targets of recording electrodes (marked by Dil) in VB. PV antibody was used to stain the reticular thalamic nuclei (RTN). (C) Representative LFP, MUA, and MUA spike raster plot during an ictal event. Magenta vertical line marks the first spike of the VB. (D) Average time of occurrence of the first spike in cortex and thalamus before the peak of the initiating slow wave of an ictal event (Wilcoxon rank sum test, $***P = 6.1 \times 10^{-15}$; $n = 50$ ictal events from five animals).

FIGURE 4: The preictal pause shares features with interictal network down states. (A) Raw LFP recording and raster plots of putative interneuron single unit (red) and putative pyramidal cell unit activity (blue) during an ictal event (arrow) and numerous interictal slow wave oscillations (for clarity arrowheads denote three slow waves). (B) Faster time base recordings of LFP and unit raster plots of the ictal event (left) and an interictal slow wave (right). (C) Left, representative spike feature plot based on principal component (PC) 1 and PC2; yellow and red clusters are putative interneuron units, and blue cluster is putative pyramidal units. Right, spike waveforms of a putative interneuron (yellow) and putative pyramidal units (blue). (D) Time histogram of the MUA firing rate for ictal and interictal events; preictal pause, interictal

down and up states are marked (time 0, peak of interictal LFP oscillation or initial ictal slow wave; bin size = 10 ms, $n = 20$ ictal and 64 interictal events). (E) Average duration of interictal down states and preictal pauses (Wilcoxon rank sum test, $P = 0.21$; $n = 63$ interictal periods and preictal pauses from four animals; *n.s.* nonsignificant). (F) Average firing rates of putative interneuron single units (left) and putative pyramidal units (right) during interictal down and up states, preictal pauses, and ictal events (Friedman test followed by post hoc Wilcoxon signed rank test with Bonferroni correction. Interneurons: $P = 3.6 \times 10^{-7}$; interictal down versus interictal up, $P = 3.7 \times 10^{-4}$; interictal up versus preictal pause, $P = 3.7 \times 10^{-4}$; preictal pause versus ictal, $P = 0.012$. Pyramidal units: $P = 7.1 \times 10^{-50}$; interictal down versus interictal up, $P = 3.3 \times 10^{-15}$; interictal up versus preictal pause, $P = 1.2 \times 10^{-14}$; preictal pause versus ictal, $P = 2.2 \times 10^{-15}$; interictal up versus ictal, $P = 4.7 \times 10^{-15}$. $*P < 0.05$, $***P < 0.001$, *n.s.* nonsignificant). (G) Firing patterns of putative interneurons (Int) and putative pyramidal (Pyr) units during interictal and ictal events. Time 0 is the peak of the interictal oscillation or the peak of the initial ictal slow wave (for F and G, $n = 17$ interneurons and 88 pyramidal units from 20 ictal and 64 interictal events).

FIGURE 5: Comparison of neocortical up states in epileptic and control rats and the occurrence of interictal up-and-down-state sequences increases toward the onset of ictal events. (A) Representative microelectrode array LFP recordings and MUA raster plot from epileptic and control animals during NREM sleep. (B) Spectrogram of the LFP recordings from the same epileptic (top, channel 14) and control (bottom, channel 13) animals in (A). The peak

with frequency between 8-15 Hz at 27 s in the control (bottom) spectrogram represents a sleep spindle. (C) Left, comparison of average MUA firing probability across the phase of slow wave oscillations in epileptic and control animals (two-sample Kolmogorov-Smirnov test, $P = 1.8 \times 10^{-43}$; $n = 2626$ MUA spikes during interictal oscillations of five epileptic animals and 2935 MUA spikes during slow waves of five control animals). Right, average number of MUA spikes at the peak of slow wave oscillations ($0-\pi/2$) (Wilcoxon rank sum test, $***P = 1.1 \times 10^{-16}$; $n = 176$ interictal oscillations from five epileptic animals and 350 slow waves from five controls; Epi, epileptic; Con, control). (D) Left, distribution of normalized HFO power in fast ripple frequency (200-500 Hz) with regard to the phase of slow wave oscillations in epileptic animals (red) and in controls (blue) (two-sample Kolmogorov-Smirnov test, $P = 5.4 \times 10^{-13}$). Right, average HFO power in fast ripple frequency at the peak of slow wave oscillations (Wilcoxon rank sum test, $*P = 0.011$; $n = 50$ interictal oscillations from five epileptic animals and 50 slow waves from five controls). **Insets below**, 300 ms of raw HFO signals. (E) Center trace - representative LFP recordings 150 s before the onset of an ictal event. **Top inset**, representative LFP and MUA raster plots during REM sleep (left) and NREM sleep (right). **Bottom inset**, spectrogram of this 150-s LFP recording. Time 0 is the ictal onset defined by the peak of initial slow wave of the ictal complex. (F) Spasm-triggered average number of down states per second defined by binned MUA counts. Red line shows the regression model 100 s before the onset of ictal events. **Inset**, average number of down states for the entire recording sessions. (G) Spasm-triggered average probability of up states defined by spectral analysis of MUA counts. **Inset**, representative 1 s of

MUA (upper trace) and raster plot (lower trace) showing up states; in this case the up state rhythmicity was 3 Hz (for **F** and **G**, $n =$ four animals with 63 ictal events; each time point is 1 s; 95% confidence intervals for all coefficient estimates of time do not contain zero; time 0 is the ictal onset). (**H**) Preictal spasm-averaged spectrogram of MUA data from one animal ($n = 17$ events).

FIGURE 6: Chemogenetic activation of infragranular pyramidal cells increases spasm counts and spasm clustering. (**A**) Low magnification confocal image showing cortical cells transfected with virus (mCherry is reporter, SMI32 is counter stain; L, layer; w.m., white matter). (**B**) Confocal imaging of pyramidal cells (SMI32 positive cells - green) and parvalbumin (PV - blue) interneurons in cortical layer Vb (arrows denote pyramidal cells). AAV reporter is mCherry - red. Scale bar: 50 μ m. (**C**) Left, representative LFP recordings of a focal seizure induced by activating somatosensory pyramidal cells with clozapine at channel 5 in a non-epileptic control animal with DREADD. Right top, channel 5 recordings in a faster time base. Right bottom, raster plot of focal seizures in this animal. (**D**) Recordings of a spontaneous epileptic spasm during baseline recordings in an epileptic animal. (**E**) Representative LFP traces of an epileptic spasm after clozapine treatment in an epileptic animal. (**F-J**) To quantify impact of clozapine treatment, daily spasm counts (nine hours per day) were obtained. Clozapine vehicle (dimethylsulfoxide, Veh) was given (i.p.) on days 1-3 of baseline recordings - on day 4 the rats were treated with clozapine (CLZ) 1.0 mg/kg or vehicle. (**F**) Clozapine treatment had no effect on spasm counts (left) or clustering (right) in an epileptic control rat without DREADD. (**G**)

Vehicle treatment on day 4 had no effect on spasm counts (left) or clustering (right) in an epileptic control rat with DREADD. **(H)** Left, in an epileptic animal with DREADD, clozapine increased spasm counts. Right, daily raster plots of spasms showing increased spasm counts and clustering on day 4. **(I)** Average spasm counts of the epileptic controls without DREADD (Epi-No DREADD), epileptic controls with DREADD but no clozapine treatment (Epi-No CLZ), and epileptic animals with DREADD and clozapine treatment (Epi-DREADD+CLZ). Clozapine increased spasm counts only in the Epi-DREADD+CLZ group (paired-sample *t*-test; **P* = 0.012; *n.s.* nonsignificant). **(J)** Average number of spasms in clusters. Clozapine increased clustering only in the Epi-DREADD+CLZ group (paired-sample *t*-test; **P* = 0.025; *n.s.* nonsignificant). For **I** and **J**, *n* = 5 in Epi-No DREADD group, 5 in Epi-No CLZ group, and 6 in Epi-DREADD+CLZ group; differences between treatments in all groups were normally distributed (Shapiro-Wilk test).

FIGURE 7: Chemogenetic activation of infragranular neocortical pyramidal cells increases LFP oscillations preictally. **(A)** Percent time that LFPs oscillate at 1-8 Hz in first two hours after vehicle (Veh) or clozapine (CLZ) treatments in epileptic animals with DREADD and epileptic control animals without DREADD (paired-sample *t*-test; ***P* = 0.0047; *n.s.* nonsignificant, *P* = 0.15; differences between treatments in all groups were normally distributed (Shapiro-Wilk test); *n* = 6 in Epileptic-DREADD group and 5 in Epileptic-No DREADD group). **(B)** Representative raw (left) and smoothed (right) spasm-triggered average oscillations in a DREADD animal after clozapine (top) and vehicle (bottom) treatments (*n* = 22 spasms after

vehicle treatment and $n = 17$ spasms after clozapine treatment; bin size = 3 s; time 0, ictal onset).

(C) Spasm-triggered average oscillations after vehicle (blue) and clozapine (red) treatments.

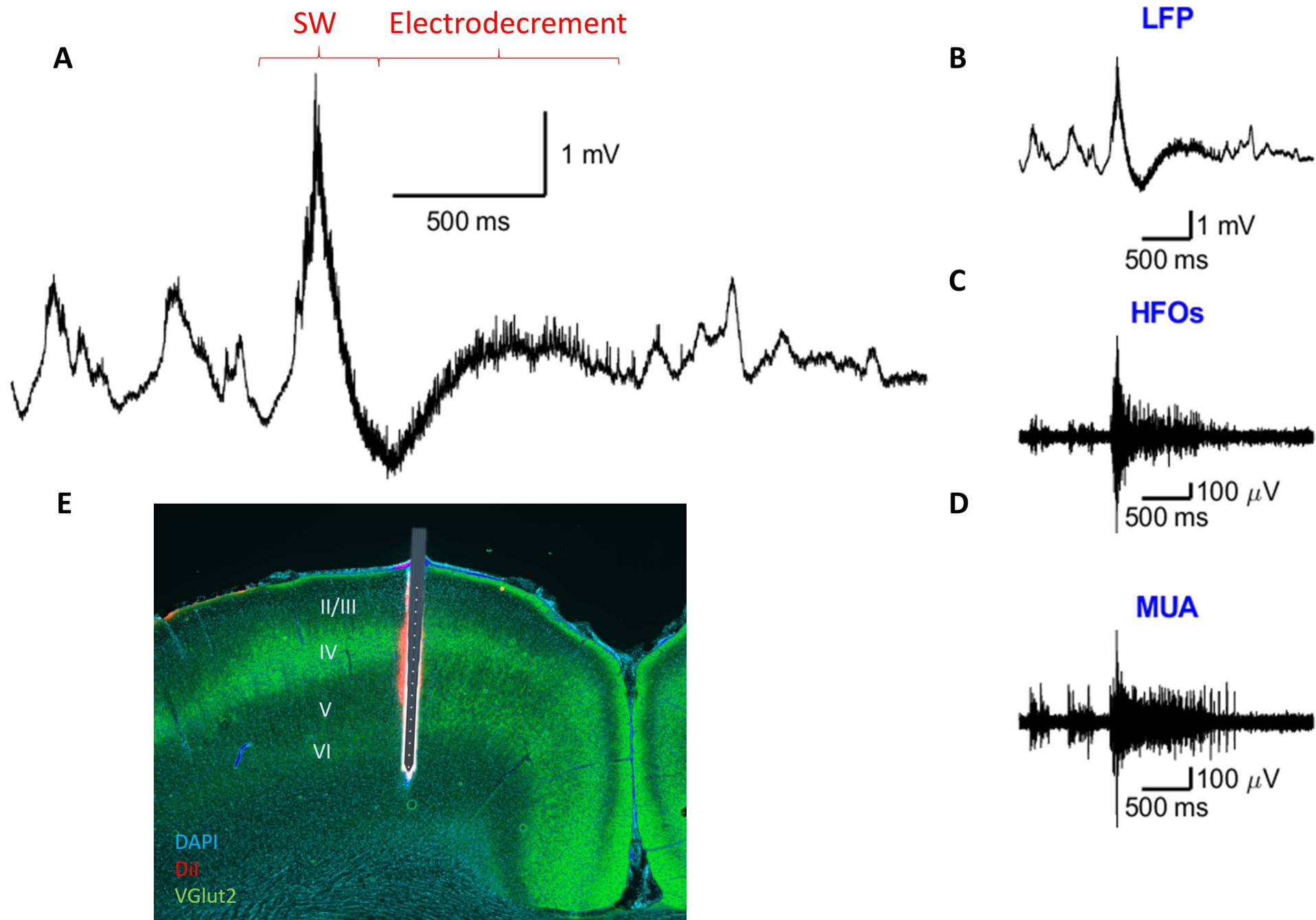
Thick blue and red curves represent the regression models 100 s before ictal events:

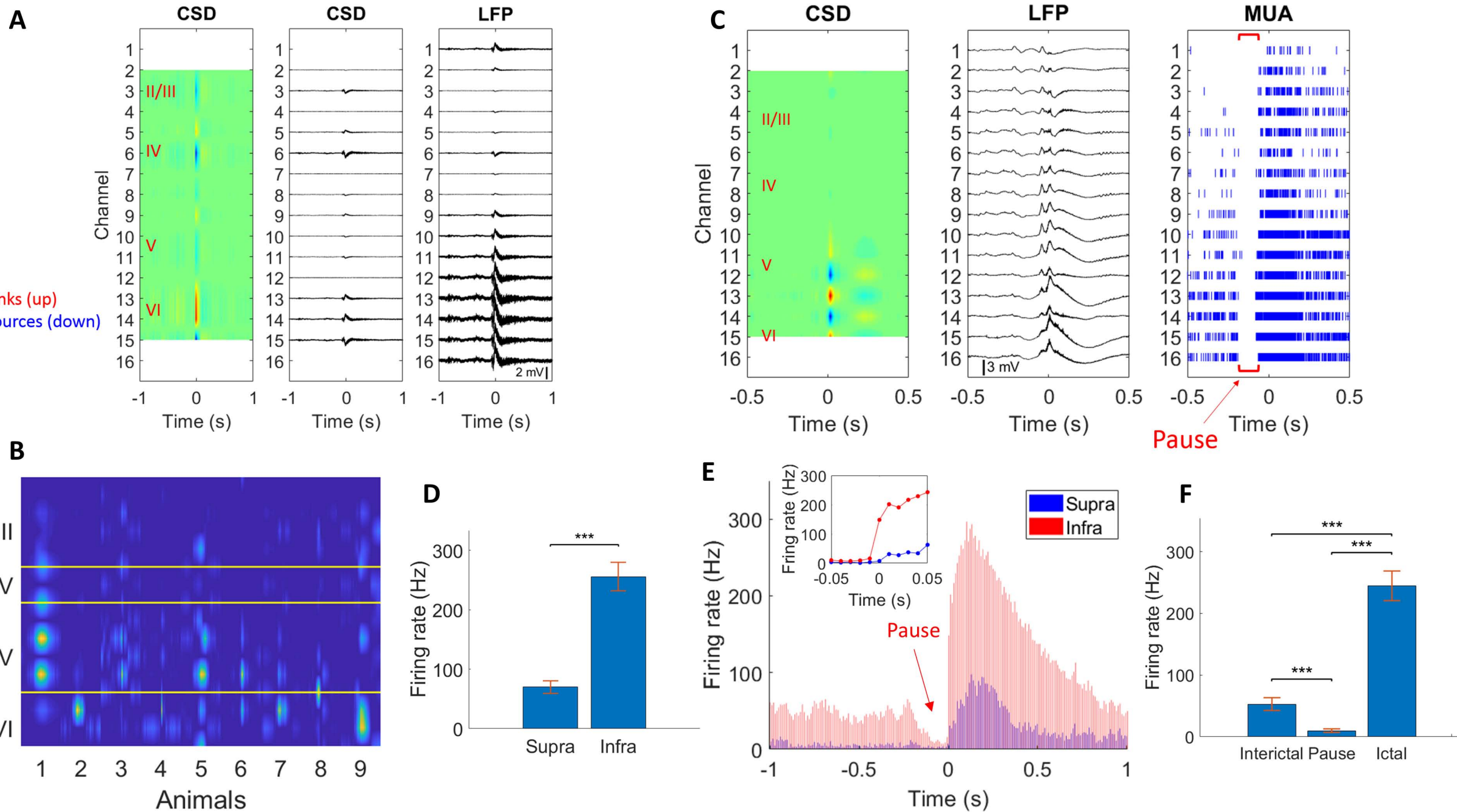
$$\text{Oscillations} = 1.49 + 0.011 \times \text{Time} + 7.0 \times 10^{-5} \times \text{Time}^2 + 0.24 \times \text{Drug}$$

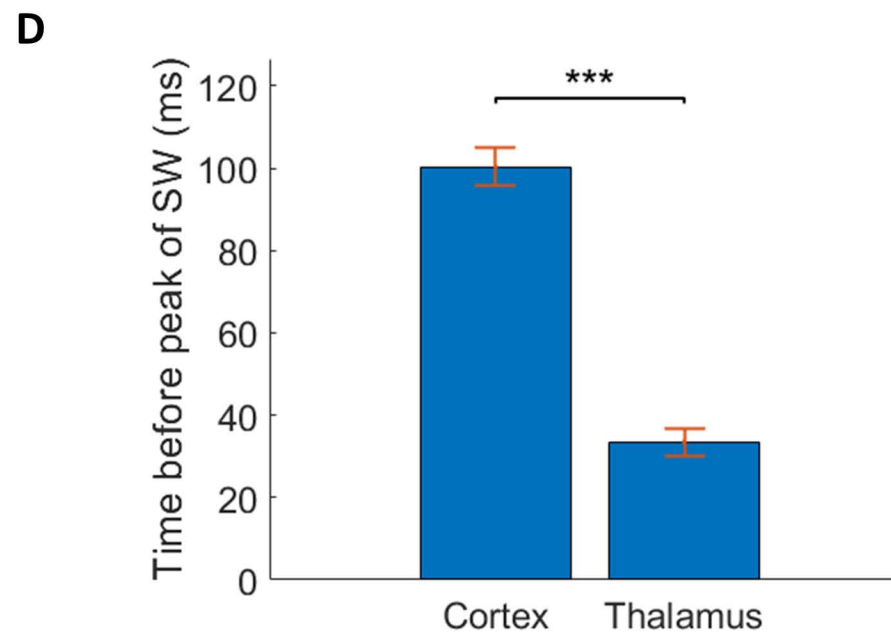
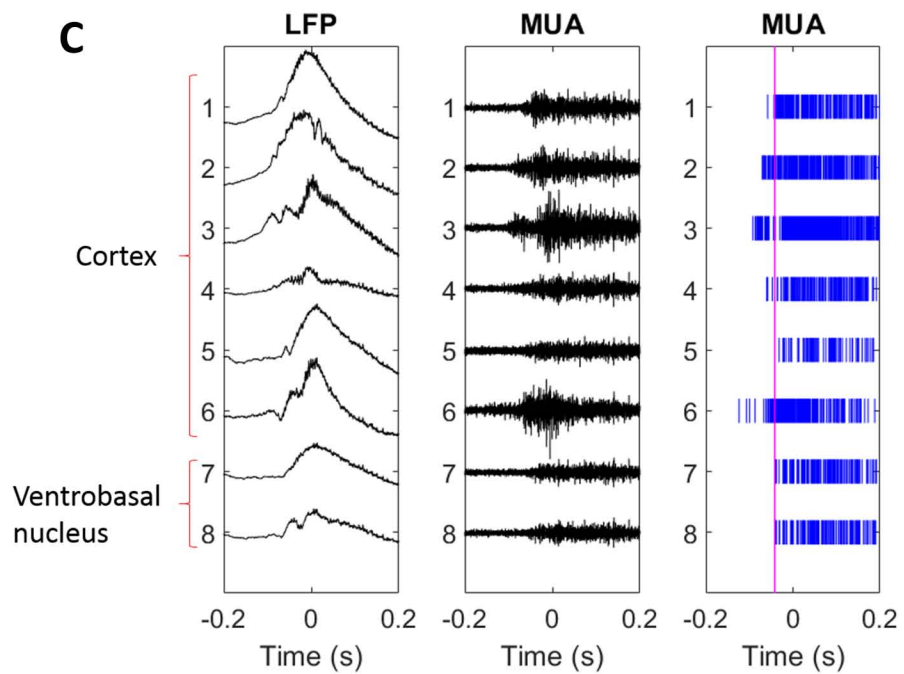
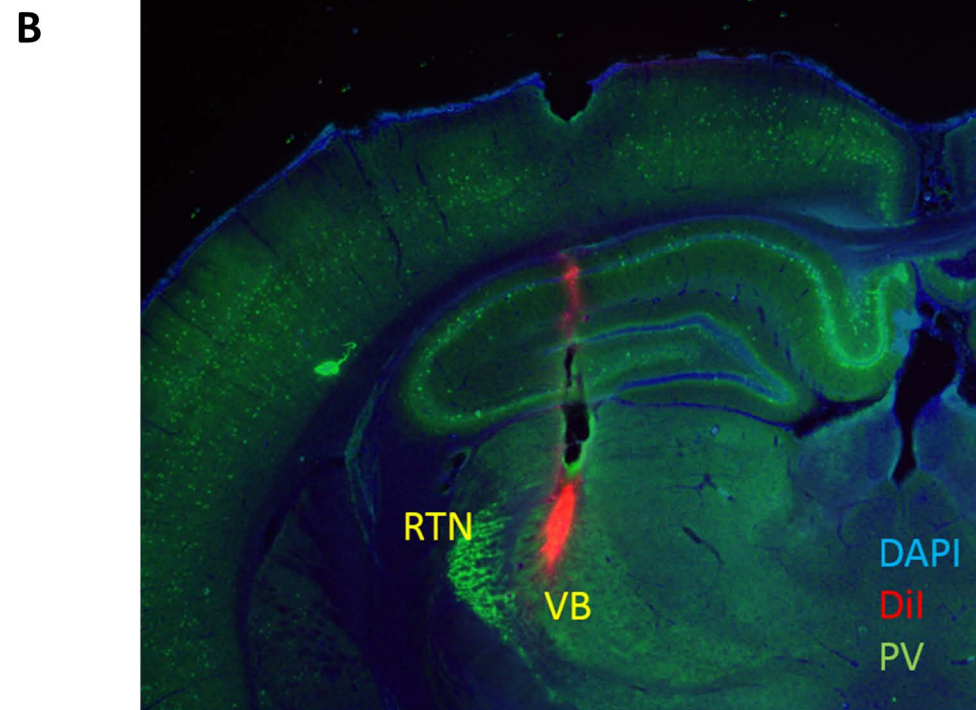
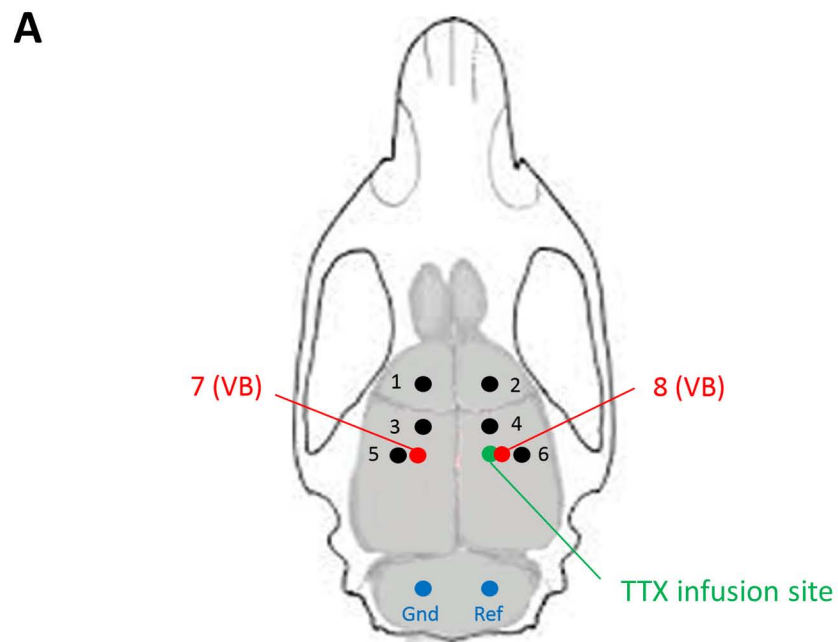
where *Drug* is either 0 (vehicle) or 1 (clozapine) and *Time* 0 is ictal onset ($n =$ six animals; bin size = 3 s; 95% confidence intervals for all coefficient estimates of *Time* and *Drug* do not contain zero). (D) Average spasm-triggered preictal spectrogram of LFP recordings after clozapine (top) and vehicle treatment (bottom) from one animal.

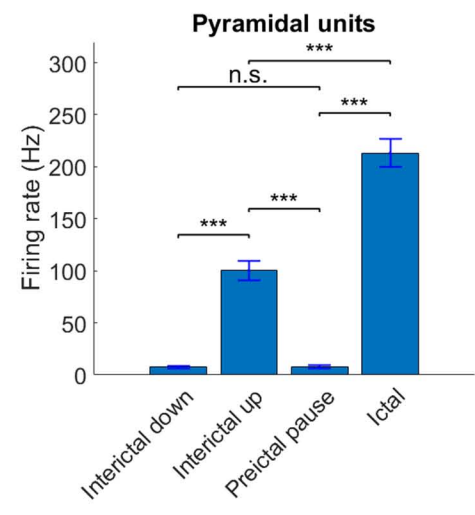
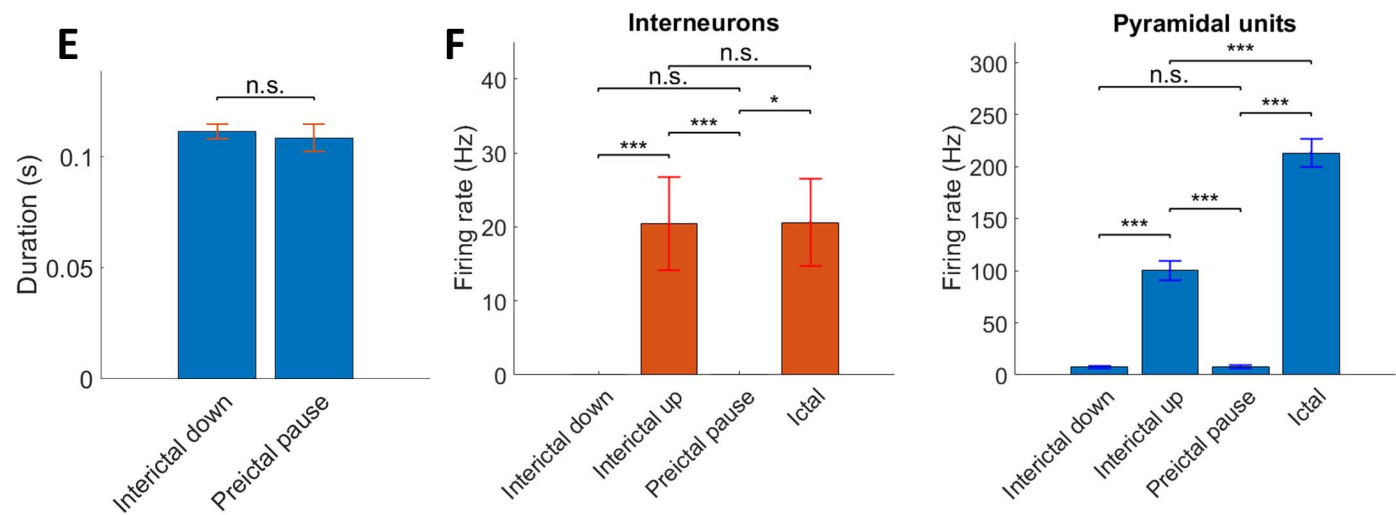
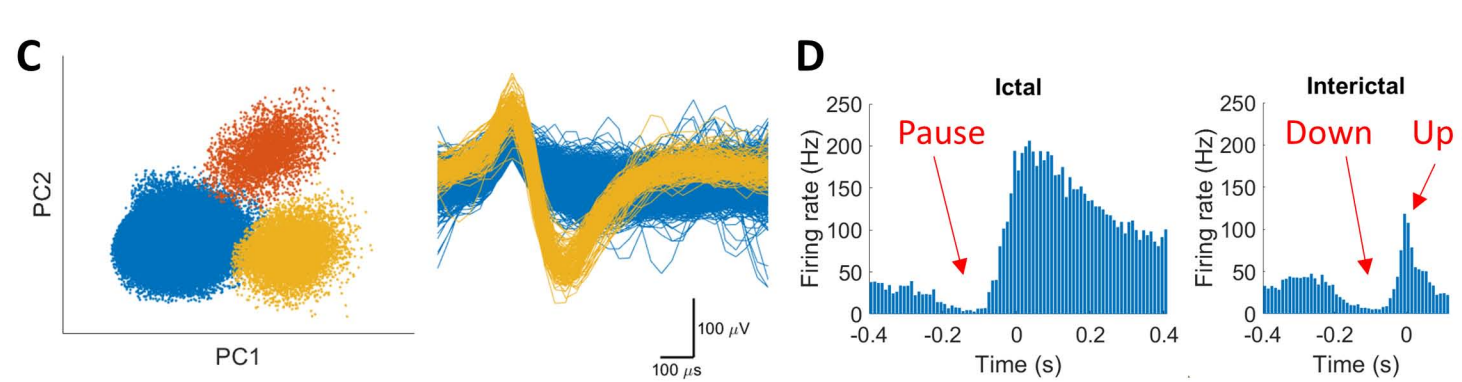
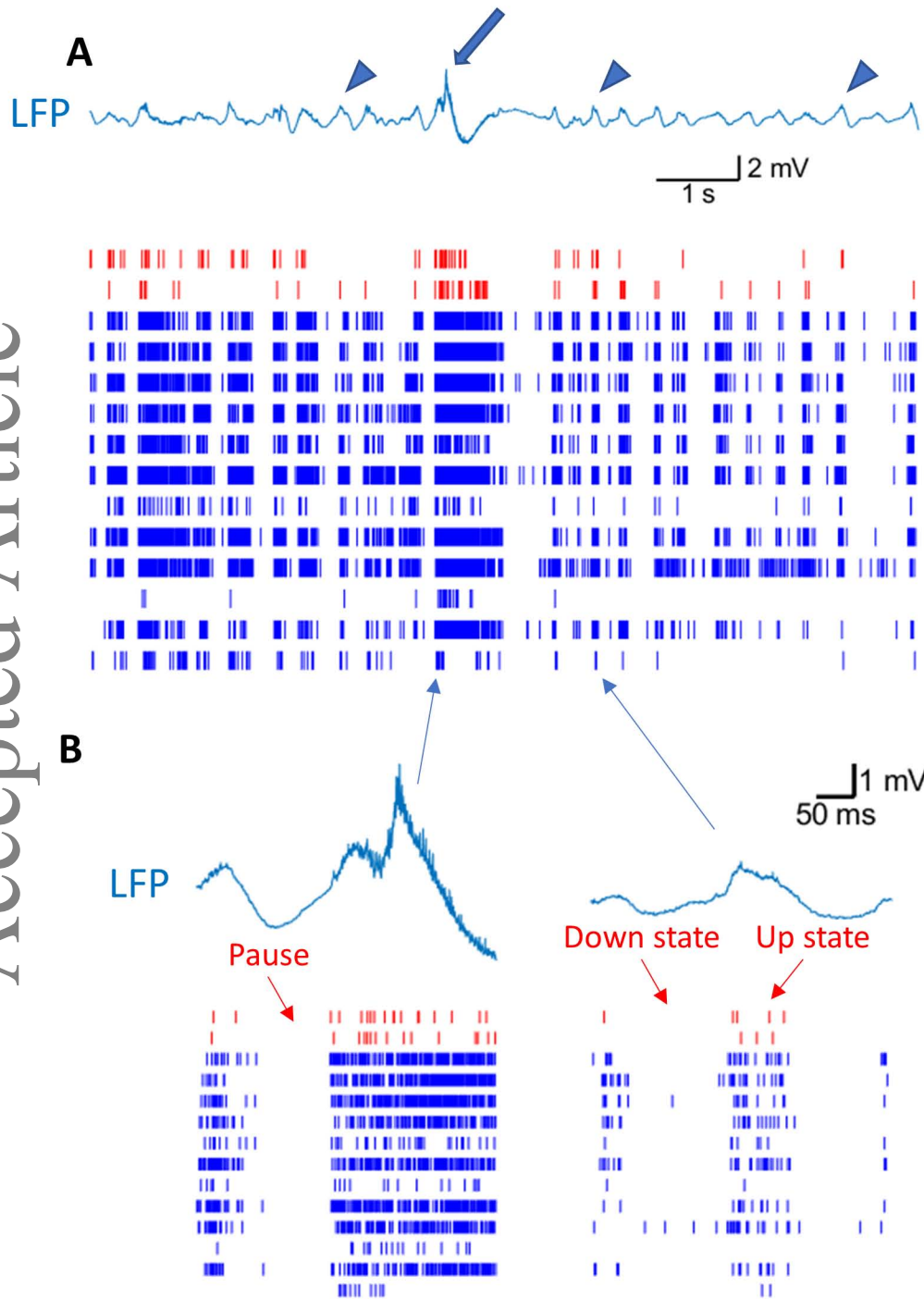
FIGURE 8: Preictal increase in LFP oscillations in patients with infantile spasms. (A)

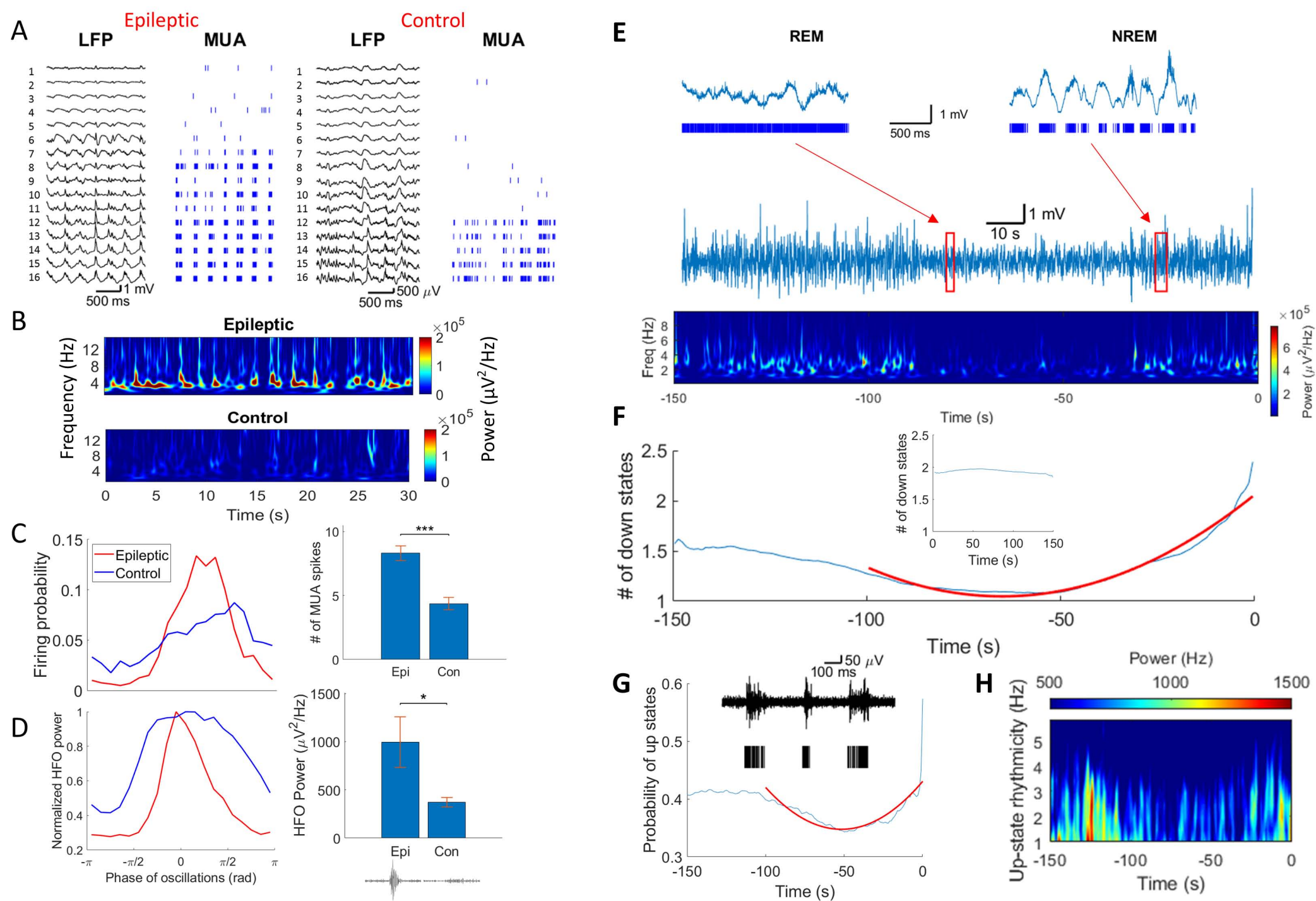
Representative preictal EEG in one patient showing increases in interictal oscillations from 50 s before the epileptic spasm (time 0). (B) Selected EEG traces at a faster time base. (C) Spasm-triggered average EEG oscillations. Red curve is the regression model ($n = 12$ ictal events from four patients; bin size = 3 s; 95% confidence intervals for all coefficient estimates of time do not contain zero; time 0, ictal onset). (D) Preictal spasm-averaged spectrogram of EEG data from one patient. (E) Average oscillations for the entire EEG recording sessions.

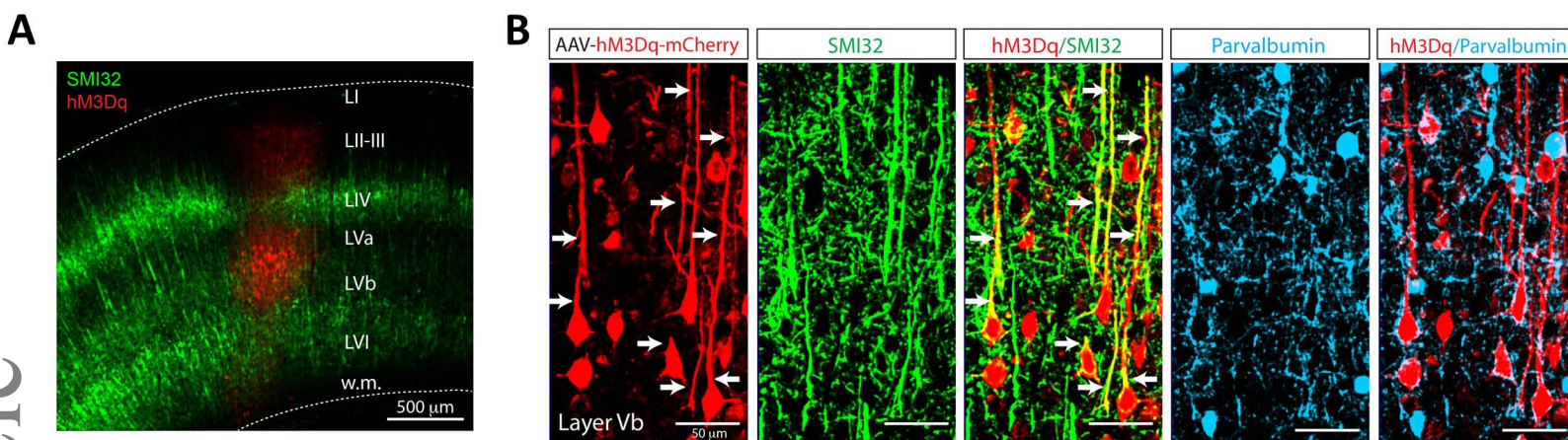




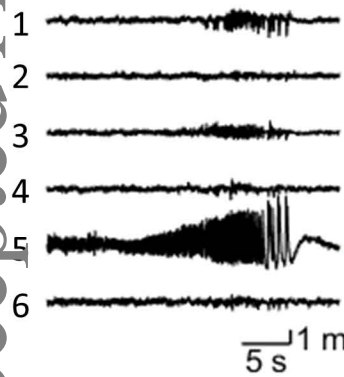






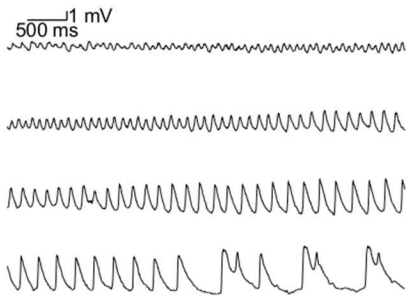


Non-epileptic-DREADD + Clozapine



1 mV
5 s

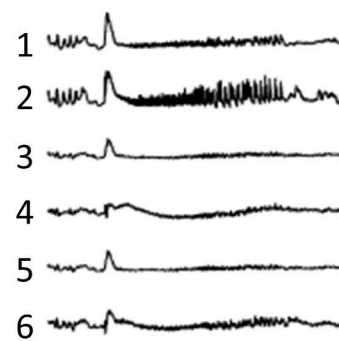
Non-epileptic-DREADD + Clozapine



1 mV
500 ms

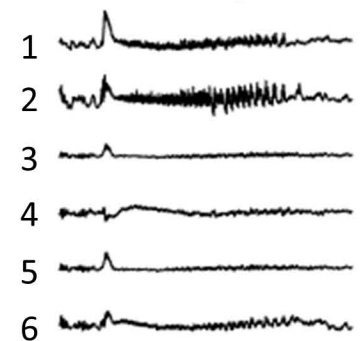
Time (min)

D Epileptic-DREADD Baseline

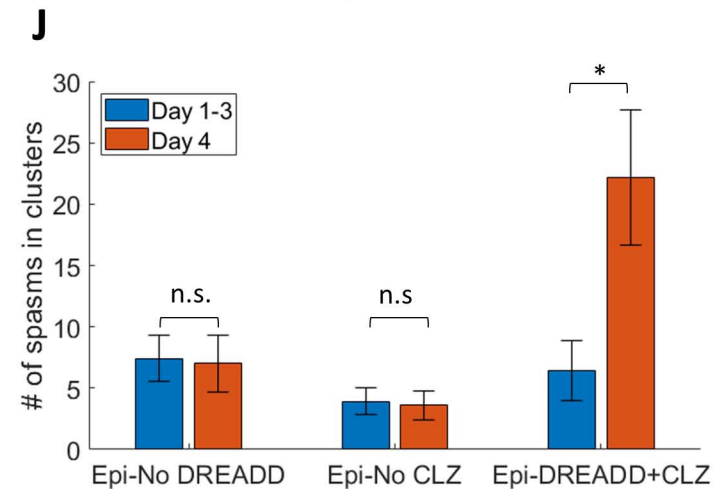
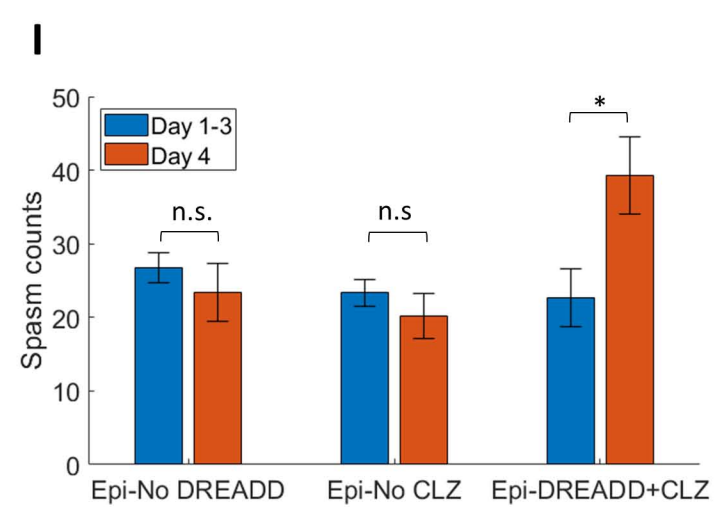


1 mV
1 s

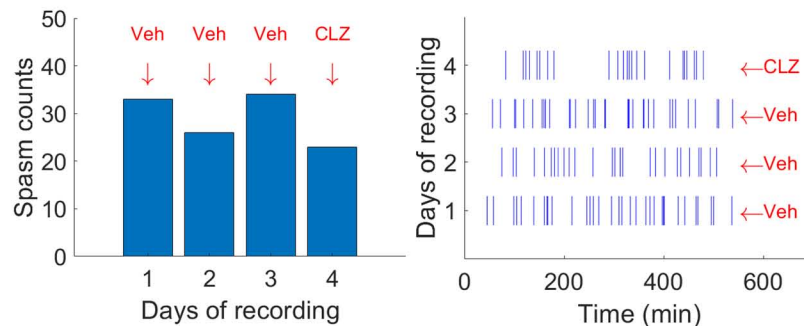
E Epileptic-DREADD + Clozapine



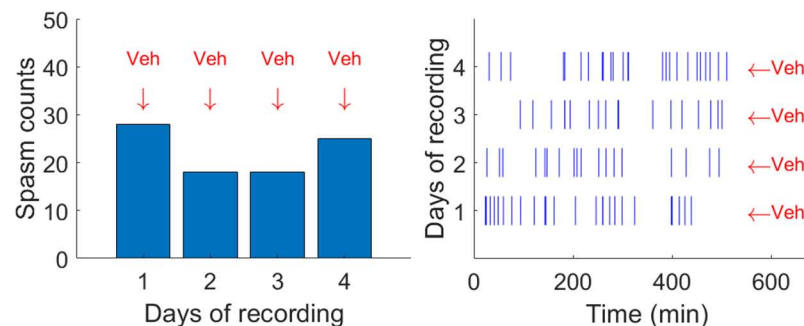
1 mV
1 s



F Epileptic-No DREADD Control



G Epileptic-No CLZ Control



H Epileptic-DREADD + Clozapine

